J. Fluid Mech. (2011), *vol.* 676, *pp.* 514–545. © Cambridge University Press 2011
doi:10.1017/jfm.2011.65

Modelling of block-scale macrodispersion as a random function

FELIPE P. J. DE BARROS[1]† AND YORAM RUBIN[2]

[1]Institute of Applied Analysis and Numerical Simulations/SimTech, University of Stuttgart, Pfaffenwaldring 7a, 705969 Stuttgart, Germany

[2]Department of Civil and Environmental Engineering, University of California, 627 Davis Hall, Berkeley, CA 94720-1710, USA

(Received 3 August 2010; revised 13 January 2011; accepted 3 February 2011; first published online 19 April 2011)

Numerical modelling of solute dispersion in natural heterogeneous porous media is facing several challenges. Amongst these we highlight the challenge of accounting for high-frequency variability that is filtered out by homogenization at the subgrid scale and the uncertainty in the dispersive flux for transport under non-ergodic conditions. These two effects when combined lead to inaccurate representation of the dispersive fluxes. We propose to compensate for this deficiency by defining a block-scale dispersion tensor and modelling it as a random space function $\mathscr{M}_{ij}$. The derived dispersion tensor is a function of several length scales and time. Grid blocks will be assigned dispersion coefficients generated from the $\mathscr{M}_{ij}$ distribution. We will show the dependence of $\mathscr{M}_{ij}$ on the spatial variability of the conductivity field, on the contaminant source size, on the travel time and on the grid-block scale. For an ergodic source, a statistically uniform conductivity field and very large grid blocks, $\mathscr{M}_{ij}$ is equal to the macrodispersion coefficients proposed by Dagan (*J. Fluid Mech.*, vol. 145, 1984, p. 151) with zero variance. For an ergodic source and non-uniform conductivity field with a finite-size grid block, $\mathscr{M}_{ij}$ approaches the model proposed by Rubin *et al.* (*J. Fluid Mech.*, vol. 395, 1999, p. 161). In both cases, $\mathscr{M}_{ij}$ is defined by its mean value with zero variance. $\mathscr{M}_{ij}$ is subject to uncertainty when the source is non-ergodic and when the grid block is defined by a finite scale. When the grid-block scale approaches zero, which means that the spatial variability is captured completely on the numerical grid, $\mathscr{M}_{ij}$ approaches zero with zero variance. In addition, we provide a complete statistical characterization of $\mathscr{M}_{ij}$ by invoking the concept of minimum relative entropy, thus providing upper bounds on the uncertainty associated with $\mathscr{M}_{ij}$.

Key words: geophysical and geological flows, mixing and dispersion, porous media

1. Introduction

Predicting flow and transport in natural porous media is difficult given the spatial heterogeneity of the hydraulic properties and our limited knowledge of the spatial distribution of these properties (see Rubin 2003). The tortuous flow patterns due to heterogeneity and our inability to fully characterize natural subsurface formations yield uncertainty of the location, spread and magnitude of the solute clouds. On this basis, the stochastic paradigm is invoked with the objective of quantifying flow and

† Email address for correspondence: felipe.debarros@simtech.uni-stuttgart.de

https://doi.org/10.1017/jfm.2011.65 Published online by Cambridge University Press

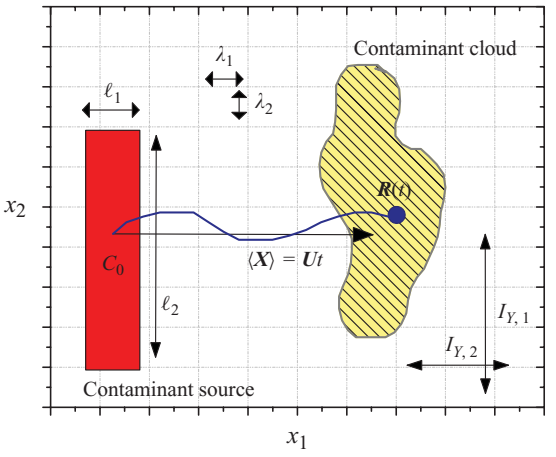


FIGURE 1. (Colour online available at journals.cambridge.org/FLM) Diagram illustrating all the relevant scales and elements affecting macrodispersion. The correlation scale of heterogeneity (or the integral scale) is denoted by $I_{Y,p}$ and the dimensions of the contaminant source are given by ℓ_p with $p = 1, \ldots, m$. In this figure, $m = 2$. Numerical grid blocks are represented by λ_p, $\boldsymbol{U}$ is the mean velocity vector, $\langle \boldsymbol{X}(t) \rangle$ is the mean displacement of the solute cloud and $\boldsymbol{R}(t)$ is the position of the cloud's centroid.

transport in natural porous media using probabilistic concepts. Such a formidable task has been a subject of numerous studies (Dagan 1984, 1987; Rubin 1990; Cvetkovic & Dagan 1994; Andricevic & Cvetkovic 1998; Cvetkovic, Dagan & Cheng 1998).

Rigorous investigation of the dispersive behaviour of solute bodies in natural porous media requires understanding the role of all relevant physical scales in the transport phenomena (e.g. Neuman 1990; Dagan 1991; Rubin *et al.* 1999). Such scales are summarized in figure 1 in a two-dimensional representation (x_1–x_2 plane). As depicted in figure 1, the initial dimensions of the solute cloud in the pth direction are given by ℓ_p with $p = 1, \ldots, m$ (where m is the space dimensionality), the dimensions of the grid block of the numerical model are denoted by λ_p and the characteristic scales of heterogeneity are represented by $I_{Y,p}$. Note that λ_p can also represent the dimension of a homogenized zone for upscaling purposes. These scales influence the location of the mean vector displacement of the solute body $\langle \boldsymbol{X}(t) \rangle$, the position of the solute cloud's centroid $\boldsymbol{R}(t)$ as well as the macrodispersion (see figure 1).

Macrodispersion tensors are developed with the aim of modelling solute transport in the context of the classical advection-dispersion equation in spatially variable velocity fields. Macrodispersion tensors account for all the effects of the unmodelled heterogeneity of the velocity field and thus can be used when the hydraulic conductivity is modelled through its effective value (Gelhar & Axness 1983; Dagan 1984, 1987; Neuman & Zhang 1990). The drawback is that the stochastic theories proposed by Gelhar & Axness (1983) and Dagan (1984) are applicable only to ergodic transport. This means that the spatial and ensemble averages are interchangeable (the solute cloud samples all the heterogeneous structure). This occurs when the characteristic dimension of the contaminant source perpendicular to the mean flow direction, for example, denoted by ℓ_2 in figure 1, is much larger than the characteristic scale of heterogeneity $I_{Y,2}$. Under ergodic transport conditions, macrodispersivities are deterministic (e.g. Dagan 1987; Rubin 2003).

When modelling solute transport numerically, one must account for the spatial variability that is not explicitly represented on the numerical grid when using grid

https://doi.org/10.1017/jfm.2011.65 Published online by Cambridge University Press

	$\lambda_p \to \infty$	Finite λ_p	$\lambda_p \to 0$
$\ell_p \to \infty$ (ergodic)	I	III	V
Finite ℓ_p (non-ergodic)	II	IV	VI

TABLE 1. Relevant length scales necessary to model macrodispersion: (I) refers to the conditions analysed by Dagan (1984), (II) refers to the conditions analysed by Dagan (1991) and (III) is the case analysed by Rubin *et al.* (1999). Cases (I), (II) and (III) were addressed before only in terms of the expected value of $\mathscr{M}_{ij}$. All cases, (I)–(VI), are addressed and investigated in this work in terms of the statistical moments of $\mathscr{M}_{ij}$.

blocks of dimensions λ_p as shown in figure 1. This variability is usually ignored which could only be justified when $\lambda_p \ll I_{Y,p}$. To address this deficiency, Rubin *et al.* (1999) introduced the concept of block-effective macrodispersion which accounts for the effects of the subgrid spatial variability that is wiped out by homogenization. In other words, the block-effective macrodispersion models the effects of the small-scale variability not represented directly on the numerical grid. The concept proposed by Rubin *et al.* (1999) was further explored and expanded in the literature (e.g. Rubin, Bellin & Lawrence 2003; Bellin, Lawrence & Rubin 2004; Eberhard 2005; Lawrence & Rubin 2007).

The complexity in defining macrodispersion tensors increases when adding into consideration the effect of non-ergodic transport (finite ℓ_2). In this case, macrodispersion depends on the source size because the spreading of a solute is controlled by local conditions (Dagan 1990; Fiori 1998; Dentz *et al.* 2000*a*, *b*), unlike the ergodic case, where local conditions are averaged out. The development of effective dispersion coefficients for non-ergodic transport was addressed in Eulerian (Kitanidis 1988) and Lagrangian (Dagan 1990, 1991) frameworks. In these works, the centroid motion of the solute cloud, denoted by $\boldsymbol{R}$ in figure 1, is regarded as uncertain and effective macrodispersion coefficients were defined in terms of an expected value. However, given that $\boldsymbol{R}$ is uncertain under non-ergodic conditions, the macrodispersion tensor (which depends on $\boldsymbol{R}$) is subject to uncertainty and must be modelled in terms of its statistical moments, or better by its statistical distribution.

In this paper, we propose to model the macrodispersion tensor as a random space function that takes into account both the dimensions of the solute cloud, ℓ_p, and of the grid block, λ_p. Considering effective macrodispersion as a random space function $\mathscr{M}_{ij}$ provides a unified framework that covers all the cases shown in table 1. Table 1 summarizes the various relationships between the relevant length scales that need to be addressed by a general macrodispersion model. As shown in table 1, for ergodic sources and uniform conductivity fields ($\ell_2 \gg I_{Y,2}$ and $\lambda_p \to \infty$, see figure 1), $\mathscr{M}_{ij}$ converges to the macrodispersion coefficients proposed by Dagan (1984). For an ergodic source and a non-uniform conductivity field ($\ell_2 \gg I_{Y,2}$ and λ_p finite, see figure 1), $\mathscr{M}_{ij}$ approaches the model proposed by Rubin *et al.* (1999) and Eberhard (2005). $\mathscr{M}_{ij}$ is subject to uncertainty when the source is non-ergodic (finite ℓ_2) and when the grid block λ_p is defined by a finite scale. When the grid-block scale approaches zero ($\lambda_p \to 0$), which means that the spatial variability is captured completely on the numerical grid, $\mathscr{M}_{ij}$ approaches zero. All these cases, as well as those in table 1 not previously addressed, are covered by the unified macrodispersion theory proposed.

https://doi.org/10.1017/jfm.2011.65 Published online by Cambridge University Press

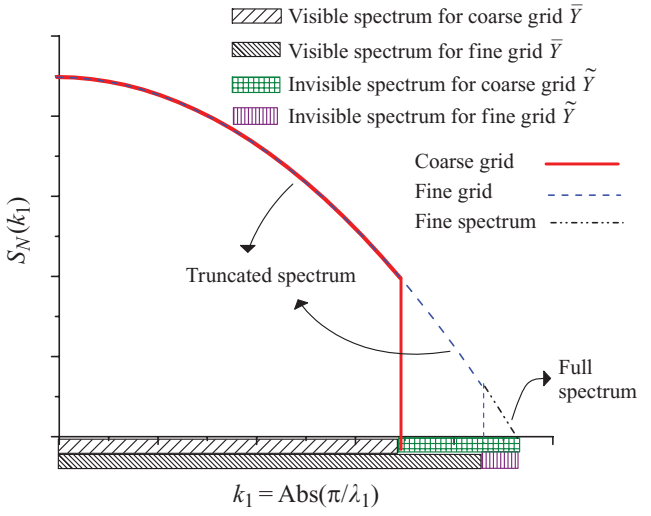


FIGURE 2. (Colour online) Corresponding visible spectra of $\overline{Y}$ for a coarse and a fine numerical grid. The wiped-out spectrum $\widetilde{Y}$, or the invisible spectrum, is also depicted. Wavenumbers are given by k_i. The shaded zones along the wavenumber axis represent the visible part of the spectrum captured over the numerical grid.

2. Theoretical fundamentals

This section presents the formulation of the block-effective macrodispersion as a random variable following the approach presented in Rubin *et al.* (1999, 2003) and generalizes it by modelling the macrodispersion tensor as a random space function. We will also show how the proposed approach provides a general framework of reference for various theories on macrodispersion.

2.1. *Scale-dependent heterogeneity and definitions*

Transport of inert solute is considered within a statistically stationary heterogeneous saturated aquifer with log–hydraulic conductivity $Y = \ln K$. Flow is incompressible at a steady state and satisfies Darcy's law. Y is characterized by its random space function parameters (Dagan 1989; Rubin 2003). It has a mean value m_Y, variance σ_Y^2, an isotropic integral scale I_Y and covariance structure C_Y. In accordance with Rubin *et al.* (1999), we separate Y into three components:

$$Y(\boldsymbol{x}) = m_Y + \overline{Y}(\boldsymbol{x}) + \widetilde{Y}(\boldsymbol{x}), \tag{2.1}$$

where $\overline{Y}$ and $\widetilde{Y}$ are the large- and small-scale fluctuations with $\langle \overline{Y} \rangle = \langle \widetilde{Y} \rangle \equiv 0$ (Rubin *et al.* 1999, 2003; Bellin *et al.* 2004). Here, the angled brackets denote ensemble expectation and $\boldsymbol{x} = (x_1, \ldots, x_m)$ is the Cartesian coordinate vector. Within a numerical modelling context, $\overline{Y}$ represents the variability captured directly on the grid block of dimension λ_p $(p = 1, \ldots, m)$, whereas $\widetilde{Y}$ stands for the subgrid-block-scale variability at a scale smaller than λ_p. This subgrid-block-scale variability is lost due to homogenization (Ababou *et al.* 1989).

A graphical representation of the visible spectrum $\overline{Y}$ captured on the numerical grid (denoted by S_N in Fourier space) for two Y fields at different resolutions is given in figure 2. The subscript N refers to the numerical grid. $S_N(\boldsymbol{k})$, with $\boldsymbol{k}$ representing the wavenumber vector, is obtained by applying a sharp cutoff filter following Nyquist's sampling theorem, see Bras & Rodríguez-Iturbe (1994) and Chap. 10 of Rubin (2003).

https://doi.org/10.1017/jfm.2011.65 Published online by Cambridge University Press

From figure 2, we observe the visible and invisible wavelengths. $S_N(\boldsymbol{k})$ is defined as the Y spectrum, $S_Y(\boldsymbol{k})$, for $k_p \leqslant \pi/\lambda_p$ and zero otherwise (see (3) of Rubin *et al.* 1999).

The subgrid fluctuation $\tilde{Y}$ is characterized by the following small-scale stationary covariance function in Fourier space:

$$\hat{C}_{\tilde{Y}}(\boldsymbol{k}) = \mathscr{F}(\boldsymbol{k};\boldsymbol{\lambda})\,\hat{C}_Y(\boldsymbol{k}), \tag{2.2}$$

$$\mathscr{F}(\boldsymbol{k};\boldsymbol{\lambda}) = \begin{cases} 0 & \text{for } |k_p| \leqslant \dfrac{\pi}{\lambda_p}, \quad p = 1, \ldots, m, \\ 1 & \text{otherwise}, \end{cases} \tag{2.3}$$

where $\mathscr{F}(\boldsymbol{k};\boldsymbol{\lambda})$ is a high-pass filter and $\hat{C}_Y(\boldsymbol{k})$ is the Fourier transform of the Y covariance with wavenumbers k_p. We selected a sharp high-pass filter; however, other alternatives can be found in the literature (see Beckie, Aldama & Wood 1996; Eberhard 2005; Lawrence & Rubin 2007). For completeness, we write the integral-transform pair that depicts the relation between $\hat{C}_Y(\boldsymbol{k})$ and $C_Y(\boldsymbol{r})$:

$$\left.\begin{aligned} C_Y(\boldsymbol{r}) &= \frac{1}{(2\pi)^{m/2}} \int_{-\infty}^{\infty} \cdots \int_{-\infty}^{\infty} \hat{C}_Y(\boldsymbol{k}) \exp[-\mathrm{i}\boldsymbol{k}\cdot\boldsymbol{r}]\,\mathrm{d}\boldsymbol{k}, \\ \hat{C}_Y(\boldsymbol{k}) &= \frac{1}{(2\pi)^{m/2}} \int_{-\infty}^{\infty} \cdots \int_{-\infty}^{\infty} C_Y(\boldsymbol{r}) \exp[\mathrm{i}\boldsymbol{k}\cdot\boldsymbol{r}]\,\mathrm{d}\boldsymbol{r}. \end{aligned}\right\} \tag{2.4}$$

In (2.4), $\boldsymbol{r}$ denotes the lag-distance vector and $\mathrm{i} = \sqrt{-1}$ is the imaginary complex unit.

Transport of an instantaneous released conservative tracer is described by the advection-dispersion equation as follows:

$$\left.\begin{aligned} \frac{\partial C}{\partial t} + \boldsymbol{u}\cdot\nabla C &= \nabla\cdot(\boldsymbol{D}_d \nabla C) \;\; \forall \boldsymbol{x} \in \Omega_d, \\ C(\boldsymbol{x}, 0) &= C_o \quad \forall \boldsymbol{x} \in \mathscr{V}_o, \end{aligned}\right\} \tag{2.5}$$

where $\boldsymbol{u}$ is the velocity field, $\boldsymbol{D}_d$ is the local pore-scale dispersion tensor, C is the concentration field that varies in space $\boldsymbol{x}$ and time t over the flow domain Ω_d. C_o is the concentration at the contaminant source of volume $\mathscr{V}_o$. The formulation given by (2.5) can be cast in the Lagrangian framework by regarding the solute cloud as a collection of particles satisfying the following equation (Dagan 1987):

$$C(\boldsymbol{x}, t) = \int_{\mathscr{V}_o} C_o(\boldsymbol{a})\,\delta[\boldsymbol{x} - \boldsymbol{X}_t(t;\boldsymbol{a})]\,\mathrm{d}\boldsymbol{a}, \tag{2.6}$$

where $\boldsymbol{X}_t$ is the total particle displacement vector and $\boldsymbol{a}$ is the initial coordinate of a solute parcel released within $\mathscr{V}_o$ at time $t_o = 0$.

The starting point of our derivation is the solute cloud's second spatial central moment denoted by S_{ij}. For an instantaneous injection over a finite volume $\mathscr{V}_o = \prod_{p=1}^{m} \ell_p$ at initial time $t_o = 0$, we can define S_{ij} using the Lagrangian formulation proposed by Dagan (1984, 1991):

$$S_{ij}(t|\ell_p) = \frac{1}{\mathscr{V}_o} \int_{\mathscr{V}_o} [X_{t,i}(t;\boldsymbol{a},\, t_o) - R_i(t)][X_{t,j}(t;\boldsymbol{a}) - R_j(t)]\,\mathrm{d}\boldsymbol{a}, \tag{2.7}$$

with

$$R_i(t) = \frac{1}{\mathscr{V}_o} \int_{\mathscr{V}_o} X_{t,i}(t;\boldsymbol{a})\,\mathrm{d}\boldsymbol{a}, \tag{2.8}$$

https://doi.org/10.1017/jfm.2011.65 Published online by Cambridge University Press

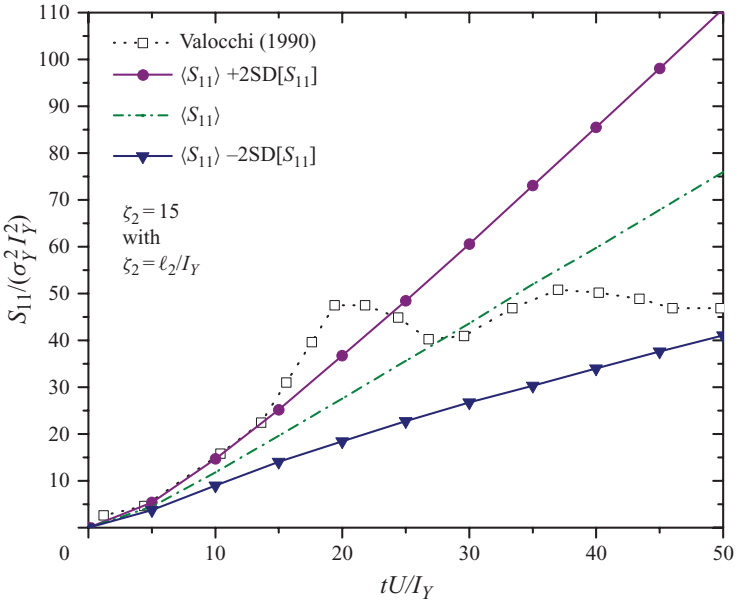


FIGURE 3. (Colour online) Temporal growth of the second central longitudinal spatial moment S_{11} as a function of the travel time for source size $\zeta_2 = 15$. Comparison between the numerical results from Valocchi (1990) and the bounds $\langle S_{11}(t)\rangle \pm 2\mathrm{SD}[S_{11}(t)]$ evaluated using the expressions given in Dagan (1990). The dimensionless transverse source size is denoted by $\zeta_2 = \ell_2/I_Y$.

where $X_{t,i}$ is the total particle displacement trajectory component in the ith direction and R_i is the centroid position vector of the solute cloud for $i = 1, \ldots, m$ (see figure 1). Equations (2.6)–(2.8) are valid in the absence of pore-scale dispersion. To account for the effects of pore-scale dispersion, the Dirac operator in (2.6) needs to be noise averaged (e.g. Risken 1989; Dagan & Fiori 1997). From (2.7), we define the 'actual' macrodispersion coefficient (in a single realization) in terms of S_{ij} for a given source:

$$D_{ij}(t|\ell_p) = \frac{1}{2}\frac{\mathrm{d}}{\mathrm{d}t}[S_{ij}(t|\ell_p)], \tag{2.9}$$

with i, j and $p = 1, \ldots, m$.

Figures 3 and 4 show two numerical simulations of $S_{ij}(t)$ from Valocchi (1990) for a single realization of the hydraulic conductivity. These numerical results are valid for a two-dimensional set-up with an isotropic exponential spatial covariance model. Figures 3 and 4 depict $S_{ij}(t)$ for transverse dimensionless source sizes $\zeta_2 = 15$ and 50 with $\zeta_2 = \ell_2/I_Y$. Based on the assumptions and conditions of Valocchi (1990), we computed the mean $\langle S_{ij}(t)\rangle$ and standard deviation $\mathrm{SD}[S_{ij}(t)]$ following the semi-analytical expressions provided in Dagan (1990) based on (2.7), see Appendix A. In these figures, we compare the numerical results with $\langle S_{ij}(t)\rangle$ and the bounds $\langle S_{ij}(t)\rangle \pm 2\ \mathrm{SD}[S_{ij}(t)]$. Comparing figures 3 with 4, we observe differences between the bounds for $S_{ij}(t)$. When the solute body approaches ergodicity ($\ell_p \gg I_Y$), $S_{ij}(t)$ is less subject to uncertainty and its bounds are tighter (compare results for $\zeta_2 = 50$ and 15). This uncertainty in $S_{ij}(t)$ is propagated to the macrodispersion coefficient by virtue of (2.9).

Summarizing, (2.9) uses the concepts introduced in Kitanidis (1988) and Dagan (1990, 1991) that incorporated the initial dimensions of the solute cloud in the

https://doi.org/10.1017/jfm.2011.65 Published online by Cambridge University Press

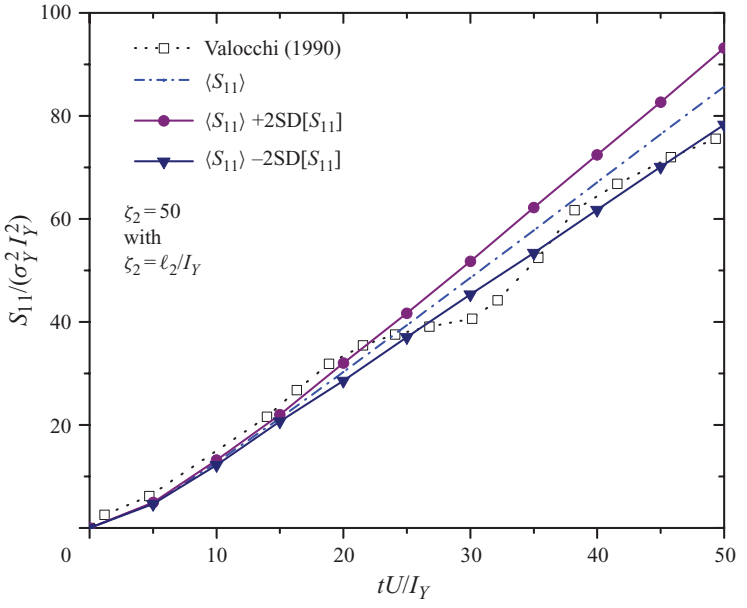


FIGURE 4. (Colour online) Temporal growth of the second central longitudinal spatial moment S_{11} as a function of the travel time for source size $\zeta_2 = \ell_2/I_Y = 50$. Comparison between the numerical results from Valocchi (1990) and the bounds $\langle S_{11}(t)\rangle \pm 2\mathrm{SD}[S_{11}(t)]$ evaluated using the expressions given in Dagan (1990). The dimensionless transverse source size is denoted by $\zeta_2 = \ell_2/I_Y$.

dispersion tensor for applications in flow and transport in porous media. Additionally, it depends on the numerical grid-block scale (Rubin *et al.* 1999, 2003). With the expansion of the range of length scales under consideration, we explore a broad range of situations and illustrate how results and cases analysed in the literature (e.g. Dagan 1984, 1990; Neuman & Zhang 1990; Dagan 1991; Rubin *et al.* 1999; Dentz *et al.* 2000*a*, *b*; Eberhard 2005) can be viewed as end-members of our proposed macrodispersion model.

2.2. *Statistical characterization of the block-effective macrodispersion tensor*

$D_{ij}(t|\ell_p)$ in (2.9) is modelled as a random space function denoted here by $\mathscr{M}_{ij}$ in order to cover all cases shown in table 1. For now, we assume that $\mathscr{M}_{ij}$ can be defined in terms of the first and second statistical moments:

$$\mathscr{M}_{ij} = F\left(\left\langle D_{ij}^{eff}(t|\ell_p, \lambda_p)\right\rangle,\ \boldsymbol{C}_D(t, t'|\ell_p, \lambda_p)\right), \tag{2.10}$$

where D_{ij}^{eff} is the block-effective dispersion tensor defined, for a given λ_p, as

$$D_{ij}^{eff}(t|\ell_p, \lambda_p) = \langle D_{ij}(t|\ell_p)\rangle_{\lambda_p}. \tag{2.11}$$

The superscript '*eff*' is now used to emphasize that we are referring to the block-effective macrodispersion tensor; thus, the dependence on λ_p becomes explicit. Moreover, the term 'effective' also refers to the fact that the macrodispersion tensor is defined in terms of an expected value over the second central spatial moment, see (2.9) and (2.10). $\langle D_{ij}^{eff}(t|\ell_p, \lambda_p)\rangle$ is the mean value and $\boldsymbol{C}_D(t, t'|\ell_p, \lambda_p)$ is the covariance tensor. In § 6, we will expand the two-moment characterization into a complete statistical characterization.

https://doi.org/10.1017/jfm.2011.65 Published online by Cambridge University Press

The first moment of the block-effective dispersion coefficient describes the actual spreading of the solute body around its centroid as follows:

$$\left\langle D_{ij}^{eff}(t|\ell_p,\lambda_p)\right\rangle = \frac{1}{2}\frac{\mathrm{d}}{\mathrm{d}t}\left\langle S_{ij}(t|\ell_p,\lambda_p)\right\rangle = \mathscr{D}_{ij}(t|\lambda_p) - r_{ij}(t|\ell_p,\lambda_p), \tag{2.12}$$

where $\mathscr{D}_{ij}(t|\lambda_p)$ is the ergodic block-effective macrodispersion coefficient that represents spreading around the mean displacement of the solute cloud and $r_{ij}(t|\ell_p,\lambda_p)$ is the variance of the solute cloud's centroid about its mean. The r_{ij} term in (2.12) represents the removal of the variability of the solute cloud's centroid following the well-known concept of relative diffusion in the field of turbulence (e.g. Batchelor 1952; Chatwin & Sullivan 1979; Fischer *et al.* 1979; Sawford 2001). Notice that, according to (2.11), $\mathscr{D}_{ij}(t|\lambda_p) = \lim_{\ell_p\to\infty}\langle D_{ij}(t|\ell_p)\rangle_{\lambda_p}$.

Under a uniform-in-the-average flow with mean velocity U_p (with $p=1,\ldots,m$) and first-order approximation, $\mathscr{D}_{ij}(t|\lambda_p)$ can be expressed in terms of the Eulerian velocity covariance in Fourier space $\hat{u}_{ij}(\boldsymbol{k})$, with $\hat{u}_{ij}$ the Fourier transform of the covariance functions, over the domain of the invisible spectrum Ω (see Rubin *et al.* 1999) and the filter defined in (2.3). The resulting expression is

$$\begin{aligned}\mathscr{D}_{ij}(t|\lambda_p) &= \frac{1}{(2\pi)^{m/2}}\int_0^t\int_\Omega \hat{u}_{ij}(\boldsymbol{k})\mathrm{e}^{-\mathrm{i}\boldsymbol{k}\cdot\boldsymbol{r}}\,\mathrm{d}\boldsymbol{k}\,\mathrm{d}t\\ &= \frac{U_qU_p}{(2\pi)^{m/2}}\int_0^t\int_{-\infty}^{\infty}\cdots\int_{-\infty}^{\infty}\left(\delta_{iq}-\frac{k_ik_q}{k^2}\right)\left(\delta_{jn}-\frac{k_jk_n}{k^2}\right)\\ &\quad\times\hat{C}_Y(\boldsymbol{k})\mathrm{e}^{-\mathrm{i}\boldsymbol{k}\cdot\boldsymbol{r}}\,\mathrm{d}\boldsymbol{k}\,\mathrm{d}t \;-\; \frac{U_qU_p}{(2\pi)^{m/2}}\int_0^t\int_{-\pi/\lambda_1}^{\pi/\lambda_1}\cdots\int_{-\pi/\lambda_m}^{\pi/\lambda_m}\\ &\quad\times\left(\delta_{iq}-\frac{k_ik_q}{k^2}\right)\left(\delta_{jn}-\frac{k_jk_n}{k^2}\right)\hat{C}_Y(\boldsymbol{k})\mathrm{e}^{-\mathrm{i}\boldsymbol{k}\cdot\boldsymbol{r}}\,\mathrm{d}\boldsymbol{k}\,\mathrm{d}t,\end{aligned} \tag{2.13}$$

with i, j, n, p and $q=1,\ldots,m$. $\hat{C}_Y(\boldsymbol{k})$ is defined in (2.4), δ_{iq} is Kronecker's delta and $k^2=\sum_{p=1}^m k_p^2$. The following relationship was used in (2.13) for the velocity covariance (see Dagan 1989):

$$\hat{u}_{ij}(\boldsymbol{k}) = U_qU_p\left(\delta_{iq}-\frac{k_ik_q}{k^2}\right)\left(\delta_{jn}-\frac{k_jk_n}{k^2}\right)\hat{C}_Y(\boldsymbol{k}). \tag{2.14}$$

The above expression assumes a steady-state flow within a stationary domain far from boundaries and free from sinks and sources. Expressions for the velocity covariance that accounts for higher order terms can be found in Hsu, Zhang & Neuman (1996). When $\lambda_p\to 0$, a fine numerical grid is implied, see figures 1 and 2, and $\mathscr{D}_{ij}(t|\lambda_p\to 0)\to 0$, following the properties of $\mathscr{F}(\boldsymbol{k};\boldsymbol{\lambda})$ in (2.3). This means that all spatial variability is being captured on the numerical grid. The term $r_{ij}(t|\ell_p,\lambda_p)$ present in (2.12) accounts for meandering of the solute cloud's centroid at the subgrid-block scale and is defined as

$$\begin{aligned}r_{ij}(t|\ell_p,\lambda_p) &= \frac{1}{2}\frac{\mathrm{d}}{\mathrm{d}t}\left[R_{ij}(t|\ell_p,\lambda_p)\right],\\ &= \frac{1}{2}\frac{\mathrm{d}}{\mathrm{d}t}\left[\frac{1}{\mathscr{V}_o^2}\int_{\mathscr{V}_o}\int_{\mathscr{V}_o} Z_{ij}(t|\boldsymbol{\beta},\lambda_p)\,\mathrm{d}\boldsymbol{a}'\,\mathrm{d}\boldsymbol{a}''\right];\quad \boldsymbol{\beta}=\boldsymbol{a}'-\boldsymbol{a}'',\end{aligned} \tag{2.15}$$

with i, j and $p=1,\ldots,m$ and $\boldsymbol{\beta}$ the spatial lag-distance. $R_{ij}(t|\ell_p,\lambda_p) = \langle R_i'(t|\ell_p,\lambda_p)R_j'(t|\ell_p,\lambda_p)\rangle$ represents the variance of the solute cloud's centroid at the subgrid-block scale. Z_{ij} denotes the two-particle covariance function (Batchelor

https://doi.org/10.1017/jfm.2011.65 Published online by Cambridge University Press

1952) and has been applied in subsurface transport (e.g. Fiori & Dagan 2000), see Appendix A for its definition. The coordinates $\boldsymbol{a}'$ and $\boldsymbol{a}''$ correspond to the initial positions of two distinct solute parcels along the injection volume $\mathscr{V}_o = \prod_{p=1}^{m} \ell_p$. Appendix B provides a more detailed version of (2.15). Substitution of (2.13) and (B 2) into (2.12) yields $\langle D_{ij}^{eff}(t|\ell_p, \lambda_p)\rangle$ as a function of the source and block dimensions, $\mathscr{V}_o = \prod_{p=1}^{m} \ell_p$ and λ_p respectively:

$$\begin{aligned}\left\langle D_{ij}^{eff}(t|\ell_p, \lambda_p)\right\rangle = {} & \frac{1}{(2\pi)^{m/2}} \int_0^t \int_{-\infty}^{\infty} \cdots \int_{-\infty}^{\infty} U_q U_p \left(\delta_{iq} - \frac{k_i k_q}{k^2}\right)\left(\delta_{jn} - \frac{k_j k_n}{k^2}\right) \\ & \times \mathscr{F}(\boldsymbol{k};\boldsymbol{\lambda})\,\hat{C}_Y(\boldsymbol{k}) \mathrm{e}^{-\mathrm{i}\boldsymbol{k}\cdot\boldsymbol{r}}\,\mathrm{d}\boldsymbol{k}\,\mathrm{d}t - \frac{1}{2\mathscr{V}_o^2}\frac{\mathrm{d}}{\mathrm{d}t}\int_{\mathscr{V}_o}\int_{\mathscr{V}_o}\int_0^t\int_0^t\int_{-\infty}^{\infty}\cdots\int_{-\infty}^{\infty} \\ & \times U_q U_p \left(\delta_{iq} - \frac{k_i k_q}{k^2}\right)\left(\delta_{jn} - \frac{k_j k_n}{k^2}\right)\mathscr{F}(\boldsymbol{k})\hat{C}_Y(\boldsymbol{k}) \\ & \times \exp[-\mathrm{i}\boldsymbol{k}\cdot(\boldsymbol{r}+\boldsymbol{\beta})]\,\mathrm{d}\boldsymbol{k}\,\mathrm{d}t'\,\mathrm{d}t''\,\mathrm{d}\boldsymbol{a}'\,\mathrm{d}\boldsymbol{a}''. \end{aligned} \tag{2.16}$$

The first term on the right-hand side is the ensemble block-scale macrodispersion (2.13), whereas the second term quantifies the sample-to-sample fluctuations of the centre of mass (as a function of the block scale and source scale). Inclusion of pore-scale dispersion in the above formulation is provided in the literature (Fiori 1996, 1998; Rubin *et al.* 1999).

For the covariance of the actual block-effective dispersion, we write

$$\boldsymbol{C}_D(t, t'|\ell_p, \lambda_p) = \langle \Upsilon(t|\ell_p, \lambda_p)\Upsilon(t'|\ell_p, \lambda_p)\rangle, \tag{2.17}$$

where

$$\Upsilon(t|\ell_p, \lambda_p) = \frac{1}{2}\frac{\mathrm{d}}{\mathrm{d}t}\mathscr{S}_f(t|\ell_p, \lambda_p), \tag{2.18a}$$

with

$$\mathscr{S}_f(t|\ell_p, \lambda_p) = S_{ij}(t|\ell_p, \lambda_p) - \langle S_{ij}(t|\ell_p, \lambda_p)\rangle. \tag{2.18b}$$

$\Upsilon(t|\ell_p, \lambda_p)$ represents the fluctuation of the block-effective macrodispersion at different travel times that the solute body will experience. To obtain the variance $\mathrm{Var}[D_{ij}^{eff}(t|\ell_p, \lambda_p)]$, we set $t = t'$ in (2.17) such that $\boldsymbol{C}_D(t, t|\ell_p, \lambda_p) \equiv \mathrm{Var}[D_{ij}^{eff}(t|\ell_p, \lambda_p)]$. The variance can be expressed as

$$\mathrm{Var}\left[D_{ij}^{eff}(t|\ell_p, \lambda_p)\right] = \left\langle D_{ij}^{eff}(t|\ell_p, \lambda_p)^2\right\rangle - \left\langle D_{ij}^{eff}(t|\ell_p, \lambda_p)\right\rangle^2, \tag{2.19}$$

with $\langle D_{ij}^{eff}(t|\ell_p, \lambda_p)\rangle$ defined in (2.16). The second moment in (2.19) is expressed as

$$\left\langle D_{ij}^{eff}(t|\ell_p, \lambda_p)^2\right\rangle = \frac{1}{4}\left\langle \left[\frac{\mathrm{d}}{\mathrm{d}t} S_{ij}(t|\ell_p, \lambda_p)\right]^2\right\rangle. \tag{2.20}$$

Equation (2.19) can be evaluated with the aid of (2.2), (2.3), (2.7) and (2.12). Explicit expressions will be provided in subsequent sections.

https://doi.org/10.1017/jfm.2011.65 Published online by Cambridge University Press

2.3. *Unified macrodispersion theory*

With (2.12) and (2.19), $\mathscr{M}_{ij}$ can be defined thus providing a unified macrodispersion theory. The term 'unified' refers to the fact that the proposed macrodispersion model provides a general framework of reference for the theories proposed by Dagan (1984, 1991), Kitanidis (1988), Neuman & Zhang (1990), Rubin *et al.* (1999), Attinger *et al.* (1999), Dentz *et al.* (2000*a*, *b*) and Eberhard (2004, 2005) using the classification provided in table 1. The models such as the those listed above could be viewed as end-members of $\mathscr{M}_{ij}$ by applying certain limits in ℓ_p and λ_p to (2.16) and (2.19). These cases are listed below.

(*a*) For the limits $\ell_p \to \infty$ and $\lambda_p \to \infty$, (2.16) converges to the case analysed by Gelhar & Axness (1983), Dagan (1984) and Neuman & Zhang (1990). The important component in ℓ_p is the one normal to the mean flow. When these limits are satisfied, S_{ij} is deterministic since the centroid position (R_i) shown in figure 1 is not subject to uncertainty. This case corresponds to the dispersion measure denoted as D_{ens} in Zavala-Sanchez, Dentz & Sanchez-Vila (2009).

(*b*) For finite ℓ_p (non-ergodic) and $\lambda_p \to \infty$, (2.16) converges to the case analysed by Kitanidis (1988) and Dagan (1990, 1991). This condition was also investigated by Rajaram & Gelhar (1993*a*,*b*), Attinger *et al.* (1999), Dentz *et al.* (2000*a*, *b*) and Eberhard (2004, 2005). It also corresponds to the dispersion measures denoted as D_{app} and D_{eff} in Zavala-Sanchez *et al.* (2009) and Dentz & Carrera (2007).

(*c*) For the limits $\ell_p \to \infty$ and finite λ_p, (2.16) is the case analysed in Rubin *et al.* (1999, 2003), Bellin *et al.* (2004), Eberhard (2005) and Lawrence & Rubin (2007).

The above limiting cases will become more evident throughout this work when (2.16) and (2.19) are reduced to simpler forms. Finally, useful cases for applications are situations where transport is non-ergodic (finite ℓ_p) and when a finite λ_p is prescribed (see table 1). In such cases, $\mathscr{M}_{ij}$ in (2.10) is uncertain and can be characterized with (2.16), (2.19) and (2.20).

3. $\mathscr{M}_{ij}$ for stratified flow

As shown in § 2, the macrodispersion tensor is a random function and needs to be statistically characterized by $\mathscr{M}_{ij}$. In this section, we derive the moments of the block-effective macrodispersion coefficient. We illustrate the dependence of the mean and variance of the block-effective macrodispersion on both the scale of homogenization and the contaminant source size for a stratified porous formation. Moreover, the limits discussed in § 2.3 and table 1 will be more evident.

3.1. *Assumptions and approximations*

Stratified flow models can be important in hydrogeology for situations where the geological medium has a layered formation (Cvetkovic & Shapiro 1989; Fiori & Dagan 2002). Results in stratified formations may also serve for benchmarking of numerical solutions and applications for short travel distances in highly anisotropic formations (see the discussion in § 3 of Indelman & Dagan 1999). We limit our analysis under the following set of assumptions and conditions.

(*a*) Steady-state flow in a three-dimensional set-up. Flow is uniform-in-the-average along the plane of stratification (x_1–x_2) in an unbounded domain with mean velocity U along the x_1 direction.

(*b*) Solutes are instantaneously released through a line source of dimension ℓ_3 along the x_3 direction normal to bedding at $x_1 = x_2 = 0$. Solute is released at the ambient velocity for each of the layers (not pressure injected). Transport is purely

https://doi.org/10.1017/jfm.2011.65 Published online by Cambridge University Press

advective (high Péclet number: $Pe \to \infty$) and under these conditions it can be viewed as two-dimensional (x_1–x_3 plane).

(*c*) Hydraulic conductivity varies in the vertical direction, $Y(x_3) = \ln[K(x_3)]$, such that the longitudinal velocity is given by $u_1(x_3) = U + u_1'(x_3)$, where u_1' is the velocity fluctuation.

(*d*) The heterogeneity of the porous media is characterized by a Gaussian covariance function $C_Y = \sigma_Y^2 \rho_Y$ with ρ_Y denoting the correlation function.

Following the work of Fiori & Dagan (2002), we have the following Y correlation structure for the stratified formation in Fourier space with vertical integral scale I_v:

$$\hat{\rho}_Y(k_3) = \sqrt{\frac{2}{\pi}} I_v \exp\left(\frac{k_3^2 I_v^2}{\pi}\right). \tag{3.1}$$

Dagan (1990) investigated the problem of flow in stratified formation to study scale-dependent longitudinal macrodispersion. This problem was also studied by Matheron & De Marsily (1980) for transport with finite Péclet numbers. Under the conditions analysed by Dagan (1990), we have the following relationships at the first-order approximation (Dagan 1990; Indelman & Dagan 1999):

$$\left.\begin{aligned} u_1' &\cong UY', \\ X_1'(t|a_3) &\cong UtY'(a_3), \\ R_1'(t) &= \frac{1}{\ell_3}\int_0^{\ell_3} X_1'(t|a_3)\,\mathrm{d}a_3, \end{aligned}\right\} \tag{3.2}$$

where Y' represents the fluctuation of the log conductivity. Under the above-mentioned assumptions, the remaining macrodispersion component is along the longitudinal direction ($i = j = 1$). The expressions provided in (3.2) lead to the following form of the two-particle covariance function Z_{11} needed to evaluate (2.15) and (2.19):

$$\left.\begin{aligned} Z_{11}(t|\beta_3) &= U^2\sigma_Y^2 t^2 \rho_Y(\beta_3), \\ \rho_Y(\beta_3) &= \frac{1}{(2\pi)^{1/2}}\int_{-\infty}^{\infty} \hat{\rho}_Y(k_3)\exp[-\mathrm{i}k_3\beta_3]\,\mathrm{d}k_3, \quad \text{with } \beta_3 = a_3' - a_3''. \end{aligned}\right\} \tag{3.3}$$

To obtain the one-particle covariance function X_{11}, we set $\beta_3 = 0$, see Appendix A.

We point out that anomalous transport behaviour may be observed for highly heterogeneous media under purely advective transport (Dagan, Fiori & Jankovic 2003; Le Borgne, Dentz & Carrera 2008; Gotovac, Cvetkovic & Andricevic 2009; Bolster *et al.* 2010, 2011). The use of dispersion tensors for anomalous transport is supported and reported extensively (e.g. Koch & Brady 1988; Cushman & Moroni 2001). Since, for demonstration, first-order approximation in the log conductivity is being used, we will limit ourselves to mildly heterogeneous porous media, and its range of applicability has been a subject of study in the literature (e.g. Bellin, Salandin & Rinaldo 1992; de Dreuzy, Beaudoin & Erhel 2007). Our purpose here is to illustrate through this example the concepts of the preceding sections and to gain physical insights.

Alternatives to perturbation methods are also available in the literature (see Dentz & Tartakovsky 2008; Fiori *et al.* 2010). The approach and concepts presented in this work are not limited to mild heterogeneity. For instance, Neuman (2006) provides a method that extends the range of applicability of perturbation techniques for high heterogeneity and such a method could be used in this work. Non-perturbative methods such as coarse graining (e.g. McComb 1990; Attinger, Dentz, & Kinzelbach 2004), renormalization theories (e.g. Majda & Kramer 1999), multi-scale

https://doi.org/10.1017/jfm.2011.65 Published online by Cambridge University Press

homogenization methods (e.g. Auriault & Adler 1995) and self-consistent closures (e.g. Kraichnan 1970; Phythian & Curtis 1978; Kramer, Majda & Vanden-Eijnden 2003; Dentz & Tartakovsky 2008) are also options that could be used to obtain the moments of macrodispersion coefficients in highly heterogeneous porous media. However, the major challenge is in the ability to relate the macrodispersion tensor to the various length scales of heterogeneity and to split their combined effects into two components: one that can be captured directly on the grid and the other through macrodispersion tensors.

3.2. *Computation of the first moment*

The computation of the first moment, $\langle D_{11}^{eff}(t)\rangle$ in (2.12), requires the evaluation of $\mathscr{D}_{11}(t|\lambda)$ and $r_{11}(t|\ell_3,\lambda)$ at the block scale λ. With the aid of the relations given by (3.2) and setting $\beta_3=0$ (meaning $a_3'\to a_3''$) in (3.3), the expression for $\mathscr{D}_{11}(t|\lambda)$ is given by

$$\begin{aligned}\mathscr{D}_{11}(t|\lambda) &= U^2\sigma_Y^2 t\left[1-\frac{1}{\sqrt{2\pi}}\int_{-\pi/\lambda}^{\pi/\lambda}\hat{\rho}_Y(k_3)\,\mathrm{d}k_3\right]\\ &= U^2\sigma_Y^2 t\left\{1-\mathrm{Erf}\left[\frac{I_v\sqrt{\pi}}{\lambda}\right]\right\}.\end{aligned}\tag{3.4}$$

Next, we must derive an expression for $r_{11}\left(t\,|\ell_3,\lambda\right)$. To achieve this task, we must write the equation of the centroid variance in the longitudinal direction with the relations provided in (3.2):

$$R_{11}(t|\ell_3,\lambda)=\frac{4U^2\sigma_Y^2t^2}{\ell_3}\int_0^{\ell_3}(\ell_3-\beta_3)\,\rho_{\tilde{Y}}(\beta_3|\lambda)\,\mathrm{d}\beta_3,\tag{3.5}$$

and differentiating (3.5) with respect to time yields (see (2.15) and Dagan 1994)

$$\frac{1}{2}\frac{\mathrm{d}}{\mathrm{d}t}\left[R_{11}(t|\ell_3,\lambda)\right]=\frac{2U^2\sigma_Y^2t}{\ell_3}\int_0^{\ell_3}(\ell_3-\beta_3)\rho_{\tilde{Y}}(\beta_3|\lambda)\,\mathrm{d}\beta_3\equiv r_{11}(t|\ell_3,\lambda).\tag{3.6}$$

Substitution of (3.4) and (3.6) into (2.12) gives

$$\begin{aligned}\left\langle D_{11}^{eff}(t|\ell_3,\lambda)\right\rangle = U^2\sigma_Y^2t&\left\{1-\mathrm{Erf}\left[\frac{I_v\sqrt{\pi}}{\lambda}\right]\right\}-\frac{2U^2\sigma_Y^2t}{\ell_3\sqrt{2\pi}}\\ &\times\left[\int_{-\infty}^{\infty}\int_0^{\ell_3}(\ell_3-\beta_3)\,\hat{\rho}_Y(k_3)\exp[-\mathrm{i}k_3\beta_3]\,\mathrm{d}k_3\,\mathrm{d}\beta_3\right.\\ &\left.-\int_{-\pi/\lambda}^{\pi/\lambda}\int_0^{\ell_3}(\ell_3-\beta_3)\,\hat{\rho}_Y(k_3)\exp[-\mathrm{i}k_3\beta_3]\,\mathrm{d}k_3\,\mathrm{d}\beta_3\right].\end{aligned}\tag{3.7}$$

Performing the integrations over β_3 and k_3, finally we have

$$\begin{aligned}\left\langle D_{11}^{eff}(t|\ell_3,\lambda)\right\rangle = U^2\sigma_Y^2t&\left\{1-\mathrm{Erf}\left[\frac{I_v\sqrt{\pi}}{\lambda}\right]\right\}-2U^2\sigma_Y^2t\\ &\times\left\{\left[\frac{I_v}{\ell_3}\mathrm{erf}\left(\frac{\sqrt{\pi}\ell_3}{2I_v}\right)+\frac{2I_v^2}{\ell_3^2\pi}\left(\exp\left[-\frac{\pi\ell_3^2}{4I_v^2}\right]-1\right)\right]\right.\\ &\left.-\frac{I_v}{\pi\ell_3^2}\int_{-\pi/\lambda}^{\pi/\lambda}\left[\frac{1-\cos(k_3\ell_3)}{k_3^2}\right]\exp\left[-\frac{I_v^2k_3^2}{\pi}\right]\mathrm{d}k_3\right\}.\end{aligned}\tag{3.8}$$

https://doi.org/10.1017/jfm.2011.65 Published online by Cambridge University Press

Taking the limit $\ell_3 \to \infty$ while keeping λ fixed, thus matching the conditions in Rubin *et al.* (1999), we have the immediate result

$$\lim_{\ell_3 \to \infty} \left\langle D_{11}^{eff}(t|\ell_3, \lambda) \right\rangle = U^2 \sigma_Y^2 t \left\{ 1 - \mathrm{Erf} \left[\frac{I_v \sqrt{\pi}}{\lambda} \right] \right\}. \tag{3.9}$$

For large source and block dimensions, we retrieve the result from the theory of Dagan (1984):

$$\lim_{(\ell_3, \lambda) \to (\infty, \infty)} \left\langle D_{11}^{eff}(t|\ell_3, \lambda) \right\rangle = U^2 \sigma_Y^2 t. \tag{3.10}$$

Another interesting limit is when $\lambda \to 0$, implying a fine numerical grid:

$$\lim_{\lambda \to 0} \left\langle D_{11}^{eff}(t|\ell_3, \lambda) \right\rangle = 0; \tag{3.11}$$

$$\lim_{(\ell_3, \lambda) \to (\infty, 0)} \left\langle D_{11}^{eff}(t|\ell_3, \lambda) \right\rangle = 0. \tag{3.12}$$

This means that the velocity variability at all wavenumbers is being captured over the numerical grid and the subgrid-block-scale macrodispersion is zero independent of whether the solute body is ergodic or not.

3.3. *Computation of the second moment*

We need to evaluate (2.19) and (2.20) under the stratified flow conditions. In order to derive an expression for $\langle (\mathrm{d}S_{11}/\mathrm{d}t)^2 \rangle$, we first need to evaluate S_{11}. At this stage, we omit λ from the notation. In subsequent steps, we will apply the cutoff filter to account for the wiped-out variability (where λ becomes explicit again). Let us start with the definition of S_{11} (see (2.7)) within a stratified domain and a line source:

$$\begin{aligned} S_{11}(t|\ell_3) &= \frac{1}{\ell_3} \int_0^{\ell_3} [X_1(t|a_3) - R_1(t)]^2 \, \mathrm{d}a_3 \\ &= \frac{1}{\ell_3} \int_0^{\ell_3} [X_1'(t|a_3) - R_1'(t)]^2 \, \mathrm{d}a_3. \end{aligned} \tag{3.13}$$

Substituting the assumptions given in (3.2) into (3.13), we obtain

$$S_{11}(t|\ell_3) = \frac{U^2 t^2}{\ell_3} \mathscr{G}(\ell_3), \tag{3.14}$$

where the auxiliary function $\mathscr{G}$ is defined as

$$\mathscr{G}(\ell_3) \equiv \int_0^{\ell_3} \left[Y'(a_3) - \frac{1}{\ell_3} \int_0^{\ell_3} Y'(a_3) \, \mathrm{d}a_3 \right]^2 \mathrm{d}a_3. \tag{3.15}$$

Substitution of (3.14) into (2.20) yields the second moment

$$\frac{1}{4} \left\langle \left(\frac{\mathrm{d}S_{11}}{\mathrm{d}t} \right)^2 \right\rangle = \frac{U^4 t^2}{\ell_3^2} \langle \mathscr{G}^2(\ell_3) \rangle. \tag{3.16}$$

Focusing on the term $\mathscr{G}^2(\ell_3)$, we have

$$\left.\begin{aligned} \mathscr{G}^2(\ell_3) &= \left\{ \int_0^{\ell_3} \left[Y'(a_3) - \frac{1}{\ell_3} \int_0^{\ell_3} Y'(a_3) \, \mathrm{d}a_3 \right]^2 \mathrm{d}a_3 \right\}^2, \\ \mathscr{G}^2(\ell_3) &= \int_0^{\ell_3} \int_0^{\ell_3} \psi(a_3) \psi(a_3'') \, \mathrm{d}a_3 \, \mathrm{d}a_3'', \end{aligned} \right\} \tag{3.17a}$$

https://doi.org/10.1017/jfm.2011.65 Published online by Cambridge University Press

with

$$\psi\,(a_3) \equiv Y'\,(a_3) - \frac{1}{\ell_3}\int_0^{\ell_3} Y'\,(a_3)\;\mathrm{d}a_3. \tag{3.17b}$$

Finally, we can rewrite (3.17*a*) as follows (see Appendix C for details):

$$\mathscr{G}^2\,(\ell_3) = \theta_1 - 2\theta_2 + \theta_3, \tag{3.18}$$

where θ_1, θ_2 and θ_3 are defined below with details given in Appendix C:

$$\left.\begin{aligned}
\theta_1 &\equiv \int_0^{\ell_3}\int_0^{\ell_3} Y'^2\left(a_3^{\mathrm{I}}\right) Y'^2\left(a_3^{\mathrm{II}}\right)\,\mathrm{d}a_3^{\mathrm{I}}\,\mathrm{d}a_3^{\mathrm{II}},\\
\theta_2 &\equiv \frac{1}{\ell_3}\int_0^{\ell_3}\int_0^{\ell_3}\int_0^{\ell_3} Y'\left(a_3^{\mathrm{I}}\right) Y'^2\left(a_3^{\mathrm{II}}\right) Y'\left(a_3^{\mathrm{III}}\right)\,\mathrm{d}a_3^{\mathrm{I}}\,\mathrm{d}a_3^{\mathrm{II}}\,\mathrm{d}a_3^{\mathrm{III}},\\
\theta_3 &\equiv \frac{1}{\ell_3^2}\int_0^{\ell_3}\int_0^{\ell_3}\int_0^{\ell_3}\int_0^{\ell_3} Y'\left(a_3^{\mathrm{I}}\right) Y'\left(a_3^{\mathrm{II}}\right) Y'\left(a_3^{\mathrm{III}}\right) Y'\left(a_3^{\mathrm{IV}}\right)\mathrm{d}a_3^{\mathrm{I}}\,\mathrm{d}a_3^{\mathrm{II}}\,\mathrm{d}a_3^{\mathrm{III}}\,\mathrm{d}a_3^{\mathrm{IV}}.
\end{aligned}\right\} \tag{3.19}$$

Substituting (3.18) into (3.16) yields

$$\frac{1}{4}\left\langle\left[\frac{\mathrm{d}}{\mathrm{d}t}S_{11}(t|\ell_3)\right]^2\right\rangle = \frac{U^4t^2}{\ell_3^2}(\langle\theta_1\rangle - 2\langle\theta_2\rangle + \langle\theta_3\rangle). \tag{3.20}$$

A major simplification of (3.20) can be achieved by assuming that the fluctuations Y' follow a Gaussian distribution (Monin & Yaglom 1975) such that the following relationship holds:

$$\begin{aligned}
\left\langle Y'\left(a_3^{\mathrm{I}}\right) Y'\left(a_3^{\mathrm{II}}\right) Y'\left(a_3^{\mathrm{III}}\right) Y'\left(a_3^{\mathrm{IV}}\right)\right\rangle &= C_Y\left(a_3^{\mathrm{I}}, a_3^{\mathrm{II}}\right) C_Y\left(a_3^{\mathrm{III}}, a_3^{\mathrm{IV}}\right)\\
&\quad + C_Y\left(a_3^{\mathrm{I}}, a_3^{\mathrm{III}}\right) C_Y\left(a_3^{\mathrm{II}}, a_3^{\mathrm{IV}}\right) + C_Y\left(a_3^{\mathrm{I}}, a_3^{\mathrm{IV}}\right) C_Y\left(a_3^{\mathrm{II}}, a_3^{\mathrm{III}}\right).
\end{aligned} \tag{3.21}$$

Applying the above assumption in (3.20) allows the computation of $\langle\theta_1\rangle$, $\langle\theta_2\rangle$ and $\langle\theta_3\rangle$. In the subsequent expressions, we will only account for the subgrid-block-scale variability (using $C_{\tilde{Y}} = \sigma_Y^2\rho_{\tilde{Y}}$ instead of $C_Y = \sigma_Y^2\rho_Y$) by making use of the filter $\mathscr{F}\,(k_3, \lambda)$ to obtain the small-scale correlation function $\rho_{\tilde{Y}}$:

$$\begin{aligned}
\rho_{\tilde{Y}}(\beta_3|\lambda) = \frac{1}{(2\pi)^{1/2}}\int_{-\infty}^{\infty}\hat{\rho}_Y\,(k_3)\exp[-\mathrm{i}k_3\beta_3]\,\mathrm{d}k_3\\
- \frac{1}{(2\pi)^{1/2}}\int_{-\pi/\lambda}^{\pi/\lambda}\hat{\rho}_Y\,(k_3)\exp[-\mathrm{i}k_3\beta_3]\,\mathrm{d}k_3,
\end{aligned} \tag{3.22}$$

with $\hat{\rho}_Y$ expressed in (3.1) and $\beta_3 = a_3^{\mathrm{I}} - a_3^{\mathrm{II}}$. Making use of the relationship between the correlation and covariance functions ($C_{\tilde{Y}} = \sigma_Y^2\rho_{\tilde{Y}}$), we have the following relations

https://doi.org/10.1017/jfm.2011.65 Published online by Cambridge University Press

for $\langle\theta_1\rangle$, $\langle\theta_2\rangle$ and $\langle\theta_3\rangle$:

$$\langle\theta_1\rangle = \sigma_Y^4 \left[\int_0^{\ell_3} \int_0^{\ell_3} \rho_{\tilde{Y}} \left(a_3^{\mathrm{I}}, a_3^{\mathrm{I}}|\lambda\right) \rho_{\tilde{Y}} \left(a_3^{\mathrm{II}}, a_3^{\mathrm{II}}|\lambda\right) \mathrm{d}a_3^{\mathrm{I}}\, \mathrm{d}a_3^{\mathrm{II}} + 2 \int_0^{\ell_3} \int_0^{\ell_3} \rho_{\tilde{Y}}^2 \left(a_3^{\mathrm{I}}, a_3^{\mathrm{II}}|\lambda\right) \mathrm{d}a_3^{\mathrm{I}}\, \mathrm{d}a_3^{\mathrm{II}} \right]; \tag{3.23a}$$

$$\langle\theta_2\rangle = \sigma_Y^4 \int_0^{\ell_3} \int_0^{\ell_3} \rho_{\tilde{Y}} \left(a_3^{\mathrm{I}}, a_3^{\mathrm{II}}|\lambda\right) \mathrm{d}a_3^{\mathrm{I}}\, \mathrm{d}a_3^{\mathrm{II}} + \frac{2\sigma_Y^4}{\ell_3} \int_0^{\ell_3} \int_0^{\ell_3} \int_0^{\ell_3} \rho_{\tilde{Y}} \left(a_3^{\mathrm{I}}, a_3^{\mathrm{II}}|\lambda\right) \rho_{\tilde{Y}} \left(a_3^{\mathrm{I}}, \boldsymbol{a}_3^{\mathrm{III}}|\lambda\right) \mathrm{d}a_3^{\mathrm{I}}\, \mathrm{d}a_3^{\mathrm{II}}\, \mathrm{d}a_3^{\mathrm{III}}; \tag{3.23b}$$

$$\langle\theta_3\rangle = \frac{3\sigma_Y^4}{\ell_3^2} \left[\int_0^{\ell_3} \int_0^{\ell_3} \rho_{\tilde{Y}} \left(a_3^{\mathrm{I}}, a_3^{\mathrm{II}}|\lambda\right) \mathrm{d}a_3^{\mathrm{I}}\, \mathrm{d}a_3^{\mathrm{II}} \right]^2. \tag{3.23c}$$

Rewriting (3.20) and making use of statistical stationarity so that (3.22) can be used, we have the final expression

$$\frac{1}{4} \left\langle \left[\frac{\mathrm{d}}{\mathrm{d}t} S_{11}(t|\ell_3, \lambda) \right]^2 \right\rangle = U^4 t^2 \sigma_Y^4 \left[\xi_0 + \frac{2}{\ell_3^2} (\xi_1 - \xi_2) - \frac{4}{\ell_3^3} \xi_3 + \frac{3}{\ell_3^4} \xi_2^2 \right], \tag{3.24a}$$

with

$$\left.\begin{aligned} \xi_0 &= \rho_{\tilde{Y}}^2(0|\lambda), \\ \xi_1 &= 2 \int_0^{\ell_3} (\ell_3 - \beta)\, \rho_{\tilde{Y}}^2(\beta_3|\lambda)\, \mathrm{d}\beta_3, \\ \xi_2 &= 2 \int_0^{\ell_3} (\ell_3 - \beta)\, \rho_{\tilde{Y}}(\beta_3|\lambda)\, \mathrm{d}\beta_3, \\ \xi_3 &= \int_0^{\ell_3} \left[\int_{-\gamma}^{\ell_3 - \gamma} \rho_{\tilde{Y}} \left(\beta_3|\lambda\right) \mathrm{d}\beta_3 \right]^2 \mathrm{d}\gamma. \end{aligned}\right\} \tag{3.24b}$$

Appendix D provides semi-closed expressions for ξ_1, ξ_2 and ξ_3. Combining (3.8) with (3.24*b*), we obtain (2.19) leading to

$$\mathrm{Var}\left[D_{11}^{eff}(t|\ell_3, \lambda)\right] = U^4 t^2 \sigma_Y^4 \left[\xi_0 + \frac{2}{\ell_3^2} (\xi_1 - \xi_2) - \frac{4}{\ell_3^3} \xi_3 + \frac{3}{\ell_3^4} \xi_2^2 \right] - \left\langle D_{11}^{eff}(t|\ell_3, \lambda) \right\rangle^2, \tag{3.25}$$

with ξ_0, ξ_1, ξ_2 and ξ_3 defined in (3.24*b*) and $\langle D_{11}^{eff}(t|\ell_3, \lambda)\rangle$ expressed in (3.8). When $\ell_3 \to \infty$, (3.25) tends to zero. In other words, for a large solute body, the macrodispersion coefficient becomes deterministic (see Dagan 1984; Rubin *et al.* 1999). Other limiting cases of interest are expressed below:

$$\lim_{\ell_3 \to \infty} \mathrm{Var}\left[D_{11}^{eff}(t|\ell_3, \lambda)\right] = 0; \tag{3.26}$$

$$\lim_{\lambda \to 0} \mathrm{Var}\left[D_{11}^{eff}(t|\ell_3, \lambda)\right] = 0. \tag{3.27}$$

4. Results and discussion

This section illustrates the mean and variance of the longitudinal block-effective macrodispersion coefficient for 2D transport in the stratified flow condition. For

https://doi.org/10.1017/jfm.2011.65 Published online by Cambridge University Press

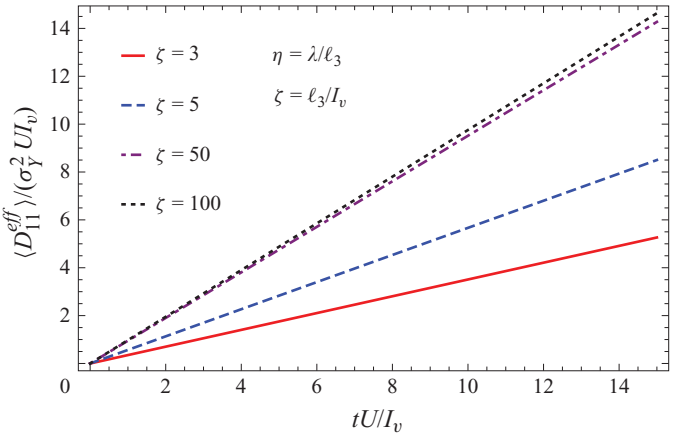


FIGURE 5. (Colour online) Expected value of the block-effective dispersion coefficient as a function of time for various source sizes $\zeta = \ell_3/I_v$. Results are given for $\eta = 1$ with $\eta = \lambda/\ell_3$.

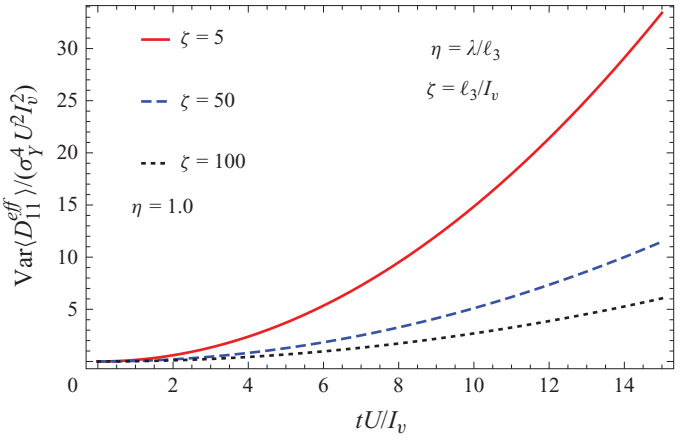


FIGURE 6. (Colour online) Dimensionless variance of the block-effective dispersion coefficient as a function of time for various plume sizes $\zeta = \ell_3/I_v$. Results are given for $\eta = 1$ with $\eta = \lambda/\ell_3$.

the plots, it is useful to define the following dimensionless quantities: $\eta = \lambda/\ell_3$ and $\zeta = \ell_3/I_v$ with η the dimensionless block size and ζ the dimensionless source size.

Figures 5 and 6 depict the first two moments of the block-effective dispersion coefficient for a block scale equal to the initial dimension of the solute body, i.e. $\eta = 1$. Figures 5 and 6 indicate that as ℓ_3 increases (thus approaching ergodicity), $\langle D_{11}^{eff}\rangle$ increases, whereas the variance decreases in line with (3.9) and (3.26). Under stratified conditions and in the absence of pore-scale dispersion, the mean and variance of the block-effective macrodispersion grow without bounds. With pore-scale dispersion or if a non-stratified formation was considered, the moments of the block-effective macrodispersion would be bounded (Fiori 1998; Fiori & Dagan 2002; Zavala-Sanchez *et al.* 2009). For a bounded stratified porous medium, the block-effective dispersion model proposed would converge to a constant asymptotic value (Zavala-Sanchez *et al.* 2009; Bolster *et al.* 2011).

Figures 7 and 8 illustrate how the mean and variance of the block-effective macrodispersion tensor behave as a function of both source and block dimensions.

https://doi.org/10.1017/jfm.2011.65 Published online by Cambridge University Press

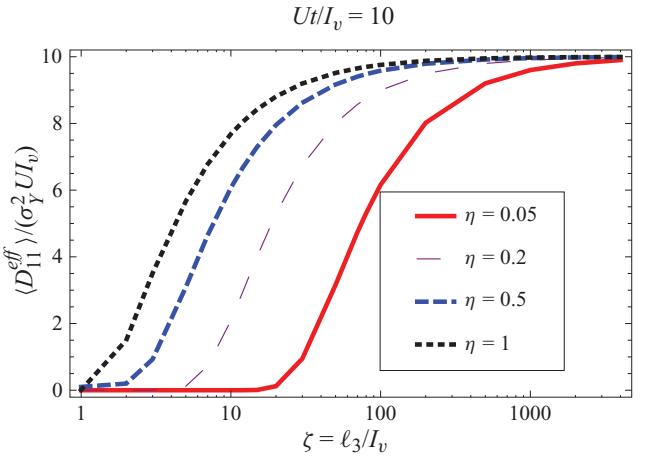


FIGURE 7. (Colour online) Mean of the block-effective dispersion coefficient as a function of the dimensionless source size ζ. Curves for $\eta = 0.05, 0.2, 0.5$ and 1. Results obtained for a fixed dimensionless time $\tau = 10$. Dimensionless parameters: $\tau = tU/I_v$, $\eta = \lambda/\ell_3$ and $\zeta = \ell_3/I_v$.

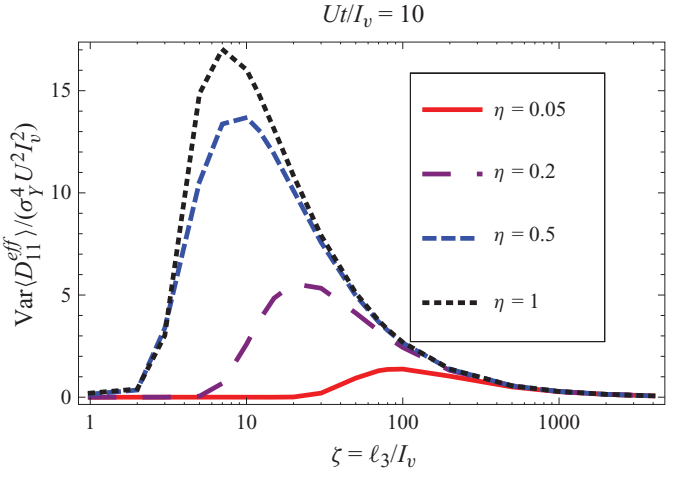


FIGURE 8. (Colour online) Variance of the block-effective dispersion coefficient as a function of the dimensionless source size ζ. Curves for $\eta = 0.05, 0.2, 0.5$ and 1. Results obtained for a fixed dimensionless time $\tau = 10$. Dimensionless parameters: $\tau = tU/I_v$, $\eta = \lambda/\ell_3$ and $\zeta = \ell_3/I_v$.

They also show the interplay between λ and ℓ_3. Figure 7 illustrates how $\langle D_{11}^{eff} \rangle$ varies with both source and block sizes at a specified time. Fixing a value for ζ, we observe that as the block size increases (larger η), there is more variability being captured at the subgrid scale, and it must be compensated for by a larger $\langle D_{11}^{eff} \rangle$. This is clearly depicted in figure 7: larger block size leads to larger values of $\langle D_{11}^{eff} \rangle$. Figure 7 also shows that as the source size ζ increases, $\langle D_{11}^{eff} \rangle$ approaches an asymptotic value that does not depend on the block size. As shown previously in figure 5, this asymptotic value is a function of time.

Figure 8 shows how the variance depends nonlinearly on ζ. This nonlinearity reflects the difference between the increase, with ζ, of the invisible spectrum, on one hand, and the approach of the invisible spectrum to ergodicity on the other hand.

https://doi.org/10.1017/jfm.2011.65 Published online by Cambridge University Press

	$\lambda_p \to \infty$	Finite λ_p	$\lambda_p \to 0$
$\ell_p \to \infty$ (ergodic)	Zero	Zero	Zero
Finite ℓ_p (non-ergodic)	Non-zero	Non-zero	Zero

TABLE 2. Cases in which the variance of the block-effective macrodispersion is equal to zero.

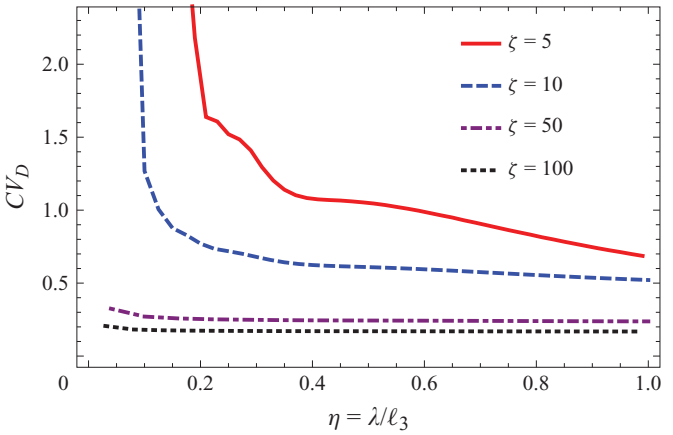


FIGURE 9. (Colour online) Coefficient of variation, $CV_D = \mathrm{SD}[D_{11}^{eff}]/\langle D_{11}^{eff}\rangle$, as a function of the block size η for different source sizes ζ. Dimensionless parameters: $\eta = \lambda/\ell_3$ and $\zeta = \ell_3/I_v$.

For small ζ, the invisible spectrum of the two different blocks can be quite different, whereas when ζ approaches ergodicity, these differences become much smaller. At very large ζ, the variance tends to zero, which means that $\langle D_{11}^{eff}\rangle$ does not depend on η and is not subject to uncertainty.

As depicted in figure 8, the variance is close to zero for small and large values of ζ. For very small ζ, the solute cloud behaves like a single particle and the effective dispersion around its centroid is practically zero. For very large ζ, the solute cloud samples the entire heterogeneous structure (ergodicity) and the second central moment tends to a deterministic quantity.

Transport is non-local (i.e. time-dependence) for all ζ, but for the mid-range ζ values, it is affected by two factors: spatial variability and the dimension of the source (see figure 5). For large ζ, the non-locality is only a factor of the spatial variability. This means that if two solute bodies with different source dimensions are released, they will experience different macrodispersion over the same block. Although somewhat counter intuitive, we recall that the block-effective macrodispersion is computed with respect to the solute cloud's centroid and not with respect to the grid-block centroid, as shown in (2.12).

Despite the nonlinear behaviour of the variance depicted in figure 8, an increase in η or ζ leads to a reduction in the coefficient of variation CV_D as shown in figure 9. An immediate observation from figure 9 is that the uncertainty is highest for smaller ζ. Moreover, as the source dimensions increase, the sensitivity of CV_D to changes in η becomes less pronounced.

With the aid of the limits investigated in (3.26) and (3.27) together with the results shown in figures 7 and 8, we can identify the conditions in which the variance of the block-effective macrodispersion is zero. These conditions are summarized in table 2.

https://doi.org/10.1017/jfm.2011.65 Published online by Cambridge University Press

5. Comparison of the unified macrodispersion theory with previous work

In this section, we will illustrate how the proposed model converges in the limits to cases analysed in the literature (see table 1). Previous cases reported in the list in § 2.3 focused on the first moment of $\mathscr{M}_{ij}$, and this will be the focus of our discussion. Consider the simple case of an isotropic two-dimensional planar flow (in the x_1–x_2 plane). Flow is steady and uniform-in-the-average along the x_1 direction with mean velocity $\boldsymbol{U} = (U, 0)$. Under the uniform-in-the-average flow condition and assuming a statistical stationary field, the one- and two-particle statistics covariances (X_{ij} and Z_{ij} respectively) can be written in terms of the Eulerian velocity covariance at first order:

$$X_{ij}(t|\boldsymbol{a}, \lambda_p, t_o) = \int_{t_o}^{t}\int_{t_o}^{t} u_{ij}(\boldsymbol{U}t|\boldsymbol{a}, \lambda_p, t_o)\,\mathrm{d}t'\,\mathrm{d}t'', \tag{5.1a}$$

$$R_{ij}(t|\ell_p, \lambda_p) = \frac{1}{\mathscr{V}_o^2}\int_{\mathscr{V}_o}\int_{\mathscr{V}_o} Z_{ij}(t|\boldsymbol{\beta}, \lambda_p,\ t_o)\,\mathrm{d}\boldsymbol{a}'\,\mathrm{d}\boldsymbol{a}'', \tag{5.1b}$$

$$Z_{ij}(t|\boldsymbol{\beta}, \lambda_p, t_o) = \int_{t_o}^{t}\int_{t_o}^{t} u_{ij}(\boldsymbol{U}t + \boldsymbol{\beta}|\boldsymbol{a}', \boldsymbol{a}'', \lambda_p, t_o)\,\mathrm{d}t'\,\mathrm{d}t'', \quad \text{with} \quad \boldsymbol{\beta} = \boldsymbol{a}' - \boldsymbol{a}'', \tag{5.1c}$$

where u_{ij} is the velocity covariance.

We consider that the underlying geostatistical structure is characterized with an isotropic Gaussian model:

$$C_Y(r_1, r_2) = \sigma_Y^2 \exp\left\{-\frac{\pi}{4}\left[\left(\frac{r_1}{I_Y}\right)^2 + \left(\frac{r_2}{I_Y}\right)^2\right]\right\}. \tag{5.2}$$

Equation (5.2) can be expressed in Fourier space as

$$\hat{C}_Y(k_1, k_2) = \frac{2\sigma_Y^2 I_Y^2}{\pi}\exp\left\{-\frac{1}{\pi}[(k_1 I_Y)^2 + (k_2 I_Y)^2]\right\}. \tag{5.3}$$

A solute is injected at time $t_o = 0$ through a line source of transverse dimension ℓ_2. For this case, we consider that advection is the dominant transport process, valid for $Pe \gtrsim 1000$ (Dagan 1989). In order to evaluate (2.12), we need to derive the case-specific expressions for (2.13) and (2.15). The first term on the right-hand side of (2.12) is

$$\mathscr{D}_{ij}(t|\lambda_1, \lambda_2, \boldsymbol{a}) = \mathscr{D}_{ij}^*(t) - \frac{U^2}{2\pi}\int_0^t \int_{-\pi/\lambda_1}^{\pi/\lambda_1}\int_{-\pi/\lambda_2}^{\pi/\lambda_2} \cos(k_1 U\tau) \times \left(\delta_{1i} - \frac{k_i k_1}{k^2}\right)\left(\delta_{1j} - \frac{k_j k_1}{k^2}\right)\hat{C}_Y(k_1, k_2)\,\mathrm{d}k_1\,\mathrm{d}k_2\,\mathrm{d}\tau, \tag{5.4}$$

where $\mathscr{D}_{ij}^*(t)$ represents the macrodispersion coefficient from the Dagan (1984) theory. For an isotropic Gaussian field, it assumes the form

$$\mathscr{D}_{ij}^*(t) = \frac{U I_Y}{\pi^2 t'^3}\left\{4 - 3\pi t'^2 + 2[\pi t'^2 - 2]\exp\left[-\frac{\pi t'^2}{4}\right] + \pi^2 t'^3 \mathrm{Erf}\left[\frac{t'\sqrt{\pi}}{2}\right]\right\}, \quad \text{with } t' = \frac{Ut}{I_Y}. \tag{5.5}$$

For the second term on the right-hand side of (2.12), we have

$$r_{ij}(t|\ell_2, \lambda_1, \lambda_2) = \frac{2}{\ell_2^2}\int_0^{\ell_2}\int_0^t (\ell_2 - \beta_2)\,u_{ij}(U\tau, \beta_2|\lambda_1, \lambda_2)\,\mathrm{d}\tau\ \mathrm{d}\beta_2, \tag{5.6}$$

https://doi.org/10.1017/jfm.2011.65 Published online by Cambridge University Press

where the dependence on λ_1 and λ_2 comes from the filter in (2.3) applied in (2.14). For the current case, the velocity covariance is given by

$$u_{ij}(U\tau, \beta_2|\lambda_1, \lambda_2) = \frac{1}{2\pi}\int_{-\infty}^{+\infty}\int_{-\infty}^{+\infty}\hat{u}_{ij}(k_1, k_2|\lambda_1, \lambda_2)\cos\left[k_1 U\tau + k_2\beta_2\right]\,\mathrm{d}k_1\,\mathrm{d}k_2. \tag{5.7}$$

Substituting (5.7) into (5.6) and integrating over t and β_2 yields

$$r_{ij}(t|\ell_2, \lambda_1, \lambda_2) = \frac{1}{\pi\ell_2^2}\int_{-\infty}^{\infty}\int_{-\infty}^{\infty}\hat{u}_{ij}(k_1, k_2|\lambda_1, \lambda_2)\vartheta(k_1, k_2, t; \ell_2, U)\,\mathrm{d}k_1\,\mathrm{d}k_2, \tag{5.8}$$

with

$$\left.\begin{aligned}
&\vartheta\,(k_1, k_2, t; \ell_2, U)\\
&\quad = \frac{\sin(k_1 Ut) + \sin(k_2\ell_2) + k_2\ell_2\cos(k_1 Ut) - \sin(k_1\ell_2 + k_1 Ut) - k_1\ell_2}{k_1 k_2^2 U};\\
&\hat{u}_{ij}(k_1, k_2|\lambda_1, \lambda_2)\\
&\quad = U^2\left(\delta_{1i} - \frac{k_i k_1}{k^2}\right)\left(\delta_{1j} - \frac{k_j k_1}{k^2}\right)\mathscr{F}(k_1, k_2|\lambda_1, \lambda_2)\hat{C}_Y(k_1, k_2).
\end{aligned}\right\} \tag{5.9}$$

Expanding (5.8), we obtain

$$\begin{aligned}
r_{ij}(t|\lambda_1, \lambda_2, \ell_2) = {}& \frac{1}{\pi\ell_2^2}\int_{-\infty}^{\infty}\int_{-\infty}^{\infty}\hat{u}_{ij}(k_1, k_2)\vartheta(k_1, k_2, t|\ell_2, U)\,\mathrm{d}k_1\,\mathrm{d}k_2\\
&-\frac{1}{\pi\ell_2^2}\int_{-\pi/\lambda_1}^{\pi/\lambda_1}\int_{-\pi/\lambda_2}^{\pi/\lambda_2}\hat{u}_{ij}(k_1, k_2)\,\vartheta(k_1, k_2, t; \ell_2, U)\,\mathrm{d}k_1\,\mathrm{d}k_2.
\end{aligned} \tag{5.10}$$

Combining (5.4), (5.5) and (5.10), we get the solution for $\langle D_{ij}^{eff}(t|\ell_2, \lambda_1, \lambda_2)\rangle$. We will consider $\lambda_1 = \lambda_2 = \lambda$ and limit our analysis to the longitudinal direction ($i = j = 1$).

Our first analysis is to confirm that the solution provided in (2.12) converges to that of Rubin *et al.* (1999) for $\ell_2 \to \infty$ and for finite λ (see table 1). For this case, we selected a large contaminant source of dimensionless size $\zeta_2 = 50$ where $\zeta_2 = \ell_2/I_Y$. Analysing figure 10, we observe that for very large block size, see the curve for $\lambda/I_Y = 20$, the mean value defined by (2.12) approaches the one provided by Dagan (1991). Moreover, as the block scale decreases ($\lambda \to 0$), more variability is captured in the numerical grid; consequently, the dispersion coefficient approaches zero, $\langle D_{ij}^{eff}(t|\ell_2, \lambda)\rangle \to 0$. Furthermore, we note that for $\zeta_2 = 50$ and finite λ, the curves computed using (2.12) are equal to those provided by Rubin *et al.* (1999).

Figure 11 shows the expected value for the block-effective macrodispersion coefficient for different dimensionless source sizes for the case with large block size ($\lambda = 50$). As shown in figure 11, our results converge to those given by the macrodispersion formulation in Dagan (1991). The reason is as follows: with increasing block size ($\lambda \to \infty$), more of the small-scale variability is being homogenized; thus, the invisible spectrum is practically equal to the full Y spectrum. This implies that all wavenumbers in the Y spectrum are folded into the block-effective macrodispersion coefficient and the only length scale that matters is the source dimension. Mathematically, the filter in (2.3) is equal to 1 and all the spectrum is assigned to the macrodispersion coefficient.

https://doi.org/10.1017/jfm.2011.65 Published online by Cambridge University Press

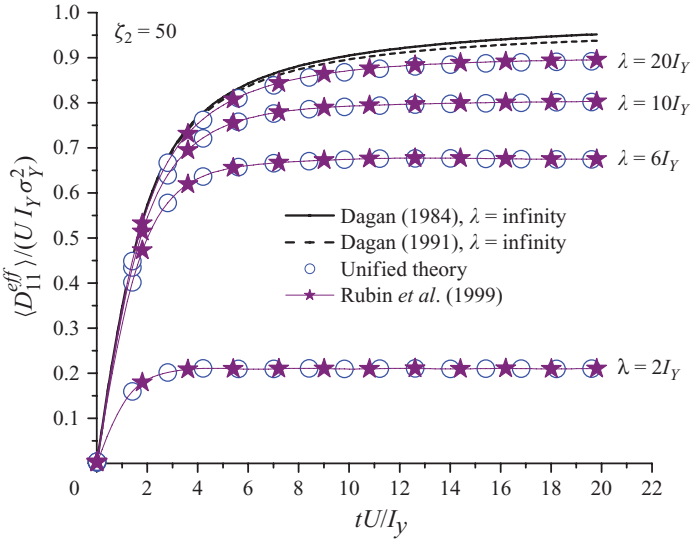


FIGURE 10. (Colour online) Convergence to the theory in Rubin *et al.* (1999). Results for an isotropic two-dimensional flow with Gaussian covariance function with dimensionless solute source size $\zeta_2 = \ell_2/I_Y = 50$, $\lambda_1 = \lambda_2 = \lambda$ and $Pe \to \infty$. The curves labelled 'unified theory' correspond to (2.12) that accounts for the theories proposed by Dagan (1991) and Rubin *et al.* (1999). Results shown for dimensionless block sizes $\lambda\ /I_Y = 2, 6, 10$ and 20.

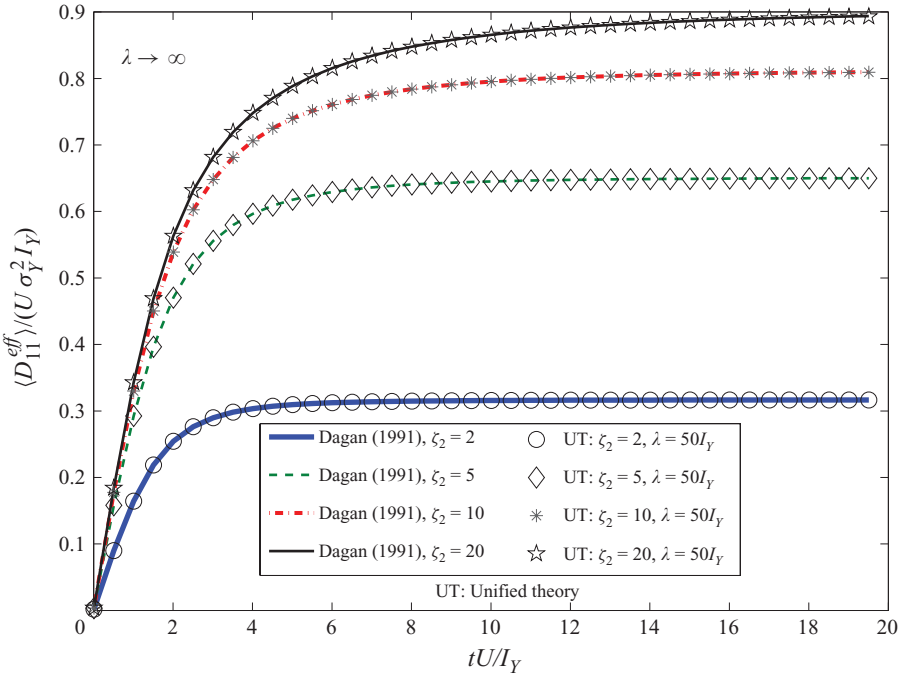


FIGURE 11. (Colour online) Convergence to the theory in Dagan (1991). Results for an isotropic two-dimensional flow with Gaussian covariance function for several contaminant source sizes $\zeta_2 = \ell_2/I_Y = 2, 5, 10$ and 20. The curves labelled 'unified theory' (UT) correspond to (2.12) that accounts for the theories proposed by Dagan (1991) and Rubin *et al.* (1999). Results shown for $\lambda = 50$ and $Pe \to \infty$.

https://doi.org/10.1017/jfm.2011.65 Published online by Cambridge University Press

6. On the probability distribution function of the macrodispersion tensor

We now wish to discuss the issue of assigning a probability density function (PDF) to the block-effective macrodispersion tensor. To address this matter, we will make use of the principle of minimum relative entropy (MRE) (Jaynes 1957; Woodbury & Ulrych 1993; Kullback 1997). We should emphasize that the MRE-based derivation of the PDF is a rational conjecture and a low-cost alternative to the derivation of the PDF from the flow and transport equations. A derivation of the PDF from the flow and transport equation is obviously expected to be more informative, and hence the MRE-based PDFs could be viewed as upper bounds on the uncertainty associated with $\mathscr{M}_{ij}$. The MRE method provides a rational approach for modelling the PDF from information that characterizes the probability distribution incompletely. Such information could be given in terms of statistical moments or bounds. The principle of MRE selects the distribution with the highest information entropy with respect to the prior information while satisfying given information allowing us to employ the model that is least subjective (see discussion in Chap. 13 of Rubin 2003).

Based on the results shown in §4, the information we have about the macrodispersion tensor is in the form of its first two moments and the condition of non-negativity which implies a lower bound equal to zero. Applying the MRE principle for this case, the prior PDF assumes the form of a truncated Gaussian PDF (Hou & Rubin 2005):

$$f_D\left(D_{ij}^{eff}\right) = \frac{\frac{1}{\sigma}\phi\left(\frac{D_{ij}^{eff}-\mu}{\sigma}\right)}{\Phi\left(\frac{b_o-\mu}{\sigma}\right)-\Phi\left(\frac{a_o-\mu}{\sigma}\right)}, \tag{6.1}$$

with a_o and b_o denoting the lower and upper bounds respectively, f_D the PDF for $D_{ij}^{eff}$and $i,\ j=1,\ldots,m$. The functions ϕ and Φ are the standard normal PDF and CDF (cumulative distribution function) respectively. The parameters μ and σ are determined from the first two moments and the bounds using the following set of equations (e.g. Hou & Rubin 2005):

$$\left\langle D_{ij}^{eff}(t|\ell_p,\lambda_p)\right\rangle = \mu + \frac{\phi\left(\frac{a_o-\mu}{\sigma}\right)-\phi\left(\frac{b_o-\mu}{\sigma}\right)}{\Phi\left(\frac{b_o-\mu}{\sigma}\right)-\Phi\left(\frac{a_o-\mu}{\sigma}\right)}\sigma\,; \tag{6.2}$$

$$\mathrm{Var}\left[D_{ij}^{eff}(t|\ell_p,\lambda_p)\right] = \sigma^2\left[1+\frac{\left(\frac{a_o-\mu}{\sigma}\right)\phi\left(\frac{a_o-\mu}{\sigma}\right)-\left(\frac{b_o-\mu}{\sigma}\right)\phi\left(\frac{b_o-\mu}{\sigma}\right)}{\Phi\left(\frac{b_o-\mu}{\sigma}\right)-\Phi\left(\frac{a_o-\mu}{\sigma}\right)}\right] - \sigma^2\left[\frac{\phi\left(\frac{a_o-\mu}{\sigma}\right)-\phi\left(\frac{b_o-\mu}{\sigma}\right)}{\Phi\left(\frac{b_o-\mu}{\sigma}\right)-\Phi\left(\frac{a_o-\mu}{\sigma}\right)}\right]^2, \tag{6.3}$$

with $i,\ j$ and $p=1,\ldots,m$.

Figures 12 and 13 illustrate the use of (6.1)–(6.3) with the results from §4. For this case, we set $a_o=0$ and $b_o\to\infty$. Figure 12 shows the impact of the block size in the PDF for $\zeta=10$. Decreasing λ (smaller η) implies that more heterogeneity is

https://doi.org/10.1017/jfm.2011.65 Published online by Cambridge University Press

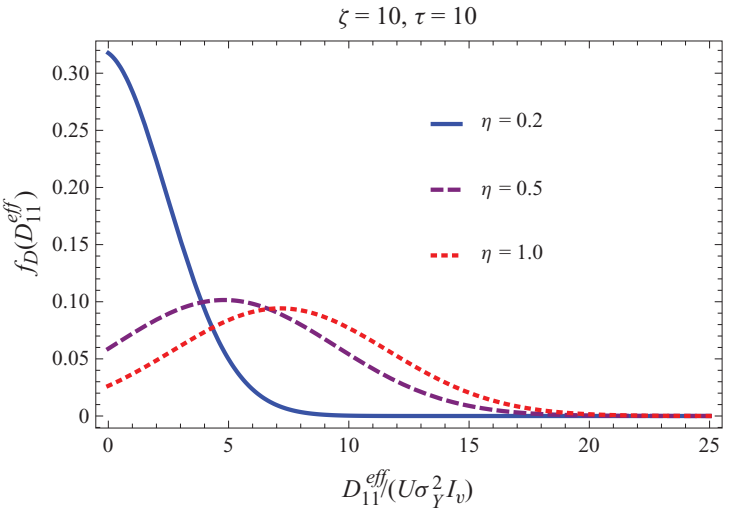


FIGURE 12. (Colour online) Illustration of the block-effective dispersion coefficient PDF for the stratified case for a source dimension $\zeta = 10$ with $\tau = 10$ as a function of $\eta = 0.2$, 0.5 and 1. Dimensionless parameters: $\tau = tU/I_v$, $\eta = \lambda/\ell_3$ and $\zeta = \ell_3/I_v$.

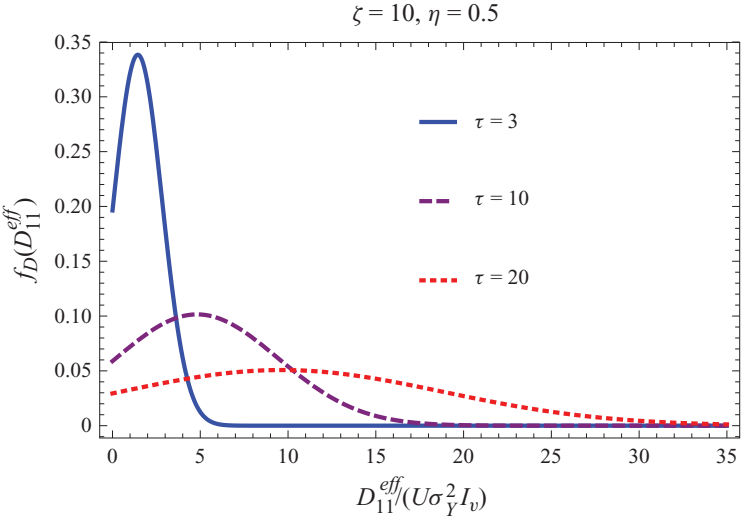


FIGURE 13. (Colour online) Illustration of the block-effective dispersion coefficient PDF for the stratified case for a source dimension $\zeta = 10$ with $\eta = 0.5$ as a function of the dimensionless time $\tau = 3$, 10 and 20. Dimensionless parameters: $\tau = tU/I_v$, $\eta = \lambda/\ell_3$ and $\zeta = \ell_3/I_v$.

being captured on the numerical grid; consequently, the variance of the block-effective dispersion decreases leading to a narrower PDF. The distributions shown in figure 12 are right skewed, which assigns larger probability to D_{11}^{eff} smaller than the expected value $\langle D_{11}^{eff} \rangle$. This is in line with the observations made by Herrera & Beckie (2009) that $\langle D_{11}^{eff} \rangle$ tends to overestimate the macrodispersion. Furthermore, it confirms the need to utilize the PDF for applications, rather than the expected value.

Figure 13 shows the PDF results as a function of time. Here we note that the PDF becomes much broader reflecting the growth in the variance with time shown in figure 6.

https://doi.org/10.1017/jfm.2011.65 Published online by Cambridge University Press

The PDF results obtained here reflect the amount of information used: first and second moments, the lower bound $a_o = 0$ and upper bound $b_o \to \infty$. The unbounded macrodispersion coefficient presented here is a consequence of transport at the infinite Péclet number condition within a stratified porous medium, see figures 5 and 6. However, for finite Péclet number, the PDFs shown in figure 12 would have upper and lower bounds (finite a_o and b_o) since the effective macrodispersion coefficient would reach an asymptotic value (e.g. Fiori 1998; Bolster, Dentz & Le Borgne 2009; Zavala-Sanchez *et al.* 2009). In a stratified formation of finite transverse extent and finite Péclet number, the effective macrodispersion reaches an asymptotic value. For an infinite transverse extent with finite Péclet number within a stratified medium, the effective macrodispersion grows without bound as $\sqrt{t}$, whereas in the infinite Péclet number case, it grows ballistically.

7. Summary

The need for modelling the uncertainty of the effective macrodispersion coefficients has been discussed in the literature (e.g. Dagan 1990, 1991), which showed the inability of dispersion coefficients obtained through ensemble averaging to model dispersion in a single realization due to variability. For early travel time, the solute body's dimensions could be of the same order as the characteristic lengths of the variability in the velocity field or smaller, and as such, the associated macrodispersion could be subject to large uncertainty that depends on the solute body's dimensions. Furthermore, in the case of numerical modelling of macrodispersion, the uncertainty in the macrodispersion is also related to the dimensions of the numerical grid blocks. In this paper we address the problem of modelling the macrodispersion of a tracer in a spatially variable velocity field and the associated uncertainty. This study focuses on macrodispersion in groundwater flow, where the variability of the velocity field is controlled by the spatial variability of the hydraulic conductivity field. However, the approach we present here could be applicable to other situations where the velocity is a random function such as in turbulent flow (e.g. Elder 1959; Chatwin & Sullivan 1979) and many types of flows taking place in open water bodies (e.g. Fischer 1973; Chatwin & Allen 1985) or in the atmosphere (e.g. Munro, Chatwin & Mole 2003; Mole, Schopflocher & Sullivan 2008).

To model the uncertainty in the rate of macrodispersion, we propose to model the macrodispersion tensor, $\mathscr{M}_{ij}$, as a random space function. This implies modelling $\mathscr{M}_{ij}$ through its statistical moments. The focus of this paper is on the first two moments of $\mathscr{M}_{ij}$. Under certain assumptions, invoking the concept of minimum relative entropy (MRE), the complete statistical distribution of $\mathscr{M}_{ij}$ can be obtained based on the first two moments and the non-negativity of $\mathscr{M}_{ij}$. The MRE-based statistical distributions provide upper bounds on the uncertainty associated with $\mathscr{M}_{ij}$.

$\mathscr{M}_{ij}$ is intended to capture the effects of the unmodelled variability of the velocity field in its entirety, i.e. the complete spectrum, such as when the flow domain is homogenized, or just in part, i.e. the part of the spectrum density that is made invisible due to homogenization, such as when some of the variability is modelled directly on a relatively coarse grid. In the latter case, $\mathscr{M}_{ij}$ captures the effects of the subgrid scale variability. To meet these goals, $\mathscr{M}_{ij}$ is modelled here as a function of the variability of the velocity field and of the various length and time scales involved, including the solute body's dimensions, the travel time and the numerical grid-block dimensions.

https://doi.org/10.1017/jfm.2011.65 Published online by Cambridge University Press

The concept underlying $\mathscr{M}_{ij}$ departs from previous works on this topic primarily on two counts. The first is the formulation of the macrodispersion tensor as a random function. Previous works on this topic (e.g. Neuman & Zhang 1990; Dagan 1991; Rubin *et al.* 1999; Dentz *et al.* 2000*a*, *b*; Eberhard 2005) focused solely on the first moment of $\mathscr{M}_{ij}$, leaving open the question of quantifying the associated uncertainty. The second count is formulation of $\mathscr{M}_{ij}$ so that it can address any portion of the spatial variability spectrum. This allows us to use $\mathscr{M}_{ij}$ in both analytical (complete spectrum becomes invisible) and numerical set-ups (only part of the spectrum becomes invisible). When considering the first moment of $\mathscr{M}_{ij}$ and for certain values of the length scales under consideration, $\mathscr{M}_{ij}$ corresponds to models derived in earlier works (e.g. Dagan 1984, 1991; Rubin *et al.* 1999; Eberhard 2005). The previous works can be viewed as end-members of the proposed model of $\mathscr{M}_{ij}$. Because $\mathscr{M}_{ij}$ bridges between previous works as well as new cases, it can be viewed as a unified theory.

Explicit, quasi-analytical expressions for $\mathscr{M}_{ij}$ are reported here for the case of advection-dominated macrodispersion within a heterogeneous, stratified formation with flow parallel to the stratification. $\mathscr{M}_{ij}$ is shown to be non-local in that its moments depend on the travel time, the solute body's dimensions and the numerical grid-block dimensions. The only case where $\mathscr{M}_{ij}$ does not depend on numerical grid-block dimensions is when the source is ergodic. Under ergodic conditions (i.e source very large in a direction normal to stratification), the first moment of $\mathscr{M}_{ij}$ is finite and is characterized by zero variance. For non-ergodic sources, $\mathscr{M}_{ij}$ has zero variance only when the grid-block dimensions approach zero, because all the variability is captured directly on the numerical grid. In this case, the first moment of $\mathscr{M}_{ij}$ is also equal to zero. In all other situations, the first moment of $\mathscr{M}_{ij}$ is subject to uncertainty. Its largest variance and coefficient of variation occur at mid-range source dimensions, of the order of 5 to 10 integral scales of the log conductivity in a direction normal to the stratification. These dimensions are of the order of the dimensions commonly encountered in situations of contamination from distributed sources, and this emphasizes the need to account for the uncertainty of the $\mathscr{M}_{ij}$.

The proposed random function model $\mathscr{M}_{ij}$ overcomes these hurdles in the sense that it expands the range of validity of the block-effective macrodispersion by accounting for all relevant length scales. In addition, $\mathscr{M}_{ij}$ quantifies the uncertainty in the macrodispersion tensor leading to a statistical characterization in terms of a PDF in which dispersion values could be assigned to grid blocks.

The ideas presented in this paper can be extended to gain further insights into mixing and dilution (Cirpka & Kitanidis 2000) since macrodispersion increases the interfacial area of the solute cloud with the surrounding fluid thus enhancing the effects of pore-scale dispersion and diffusion. Therefore, capturing the effect of sub-scale variability on transport will have an impact on the uncertainty related to mixing and dilution of tracers and reactive contaminants.

We acknowledge the comments and suggestions made by our reviewers. The first author would like to thank the German Research Foundation (DFG) for the financial support of the project within the Cluster of Excellence in Simulation Technology (EXC 310/1) at the University of Stuttgart. This study has been funded by the US DOE Office of Biological and Environmental Research, Environmental Remediation Science Program (ERSP), through DOEERSP grant DEFG0206ER0616 as part of Hanford 300 Area Integrated Field Research Challenge Project.

https://doi.org/10.1017/jfm.2011.65 Published online by Cambridge University Press

Appendix A

A.1. *Mean and variance of the second spatial moment*

Assuming normally distributed displacements for the solute particles, we have the following expressions for the mean and variance of the second spatial moment S_{ij} necessary to construct figures 3 and 4, see Dagan (1990):

$$\begin{aligned}\langle S_{11}(t)\rangle &= X_{11}(t) - \frac{1}{\mathscr{V}_o^2}\int_{\mathscr{V}_o}\int_{\mathscr{V}_o} Z_{11}(t|\boldsymbol{a}' - \boldsymbol{a}'')\,\mathrm{d}\boldsymbol{a}'\,\mathrm{d}\boldsymbol{a}'' + 2D_{d,11}t \\ &= X_{11}(t) - R_{11}(t) + 2D_{d,11}t \end{aligned} \tag{A 1}$$

and

$$\begin{aligned}\mathrm{Var}\,[S_{11}(t)] = 2R_{11}^2(t) &+ \frac{2}{\mathscr{V}_o^2}\int_{\mathscr{V}_o}\int_{\mathscr{V}_o} Z_{11}^2(t|\boldsymbol{a}' - \boldsymbol{a}'')\,\mathrm{d}\boldsymbol{a}'\,\mathrm{d}\boldsymbol{a}'' \\ &- \frac{4}{\mathscr{V}_o^3}\int_{\mathscr{V}_o}\int_{\mathscr{V}_o}\int_{\mathscr{V}_o} Z_{11}(t|\boldsymbol{a}' - \boldsymbol{a}'')Z_{11}(t|\boldsymbol{a}'' - \boldsymbol{a}''')\,\mathrm{d}\boldsymbol{a}'\,\mathrm{d}\boldsymbol{a}''\,\mathrm{d}\boldsymbol{a}'''. \end{aligned} \tag{A 2}$$

A.2. *One- and two-particle displacement covariance functions*

The two-particle covariance $Z_{ij} = \langle X_i'(t;\boldsymbol{a}', t_o)\; X_j'(t;\boldsymbol{a}'', t_o)\rangle$ is given (at first order) by (see Fiori & Dagan 2000)

$$Z_{ij}(t|\boldsymbol{a}' - \boldsymbol{a}'', Pe) = \frac{1}{(2\pi)^{m/2}}\int_0^t\int_0^t\int_{\boldsymbol{k}} u_{ij}(\boldsymbol{k})\mathscr{P}_1(t', t'', \boldsymbol{k}|\boldsymbol{a}' - \boldsymbol{a}'', Pe)\,\mathrm{d}\boldsymbol{k}\,\mathrm{d}t'\,\mathrm{d}t'', \tag{A 3}$$

with

$$\begin{aligned}\mathscr{P}_1(t', t'', \boldsymbol{k}|\boldsymbol{a}' - \boldsymbol{a}'', Pe) = \exp[-\mathrm{i}\boldsymbol{k}(\boldsymbol{a}' - \boldsymbol{a}'')]\exp[-\mathrm{i}\boldsymbol{k}\boldsymbol{U}(t' - t'')] \\ \times \exp[-k_p k_m D_{d,pm}(t' - t'')], \end{aligned} \tag{A 4}$$

where $D_{d,pm}$ is a pore-scale dispersion tensor. As for the one-particle displacement covariance function $X_{ij} = \langle X_i'(t;\boldsymbol{a}, t_o)\; X_j'(t;\boldsymbol{a}, t_o)\rangle$, we have (at first order) the following expression (e.g. Dagan 1987; Fiori & Dagan 2000):

$$X_{ij}(t|Pe) = \frac{1}{(2\pi)^{m/2}}\int_0^t\int_0^t\int_{\boldsymbol{k}} u_{ij}(\boldsymbol{k})\mathscr{P}_2(t', t'', \boldsymbol{k}|Pe)\,\mathrm{d}\boldsymbol{k}\,\mathrm{d}t'\,\mathrm{d}t'' \tag{A 5}$$

$$\mathscr{P}_2(t', t'', \boldsymbol{k}|Pe) = \exp[-\mathrm{i}\boldsymbol{k}\boldsymbol{U}(t' - t'')]\exp[-k_p k_m D_{d,pm}|t' - t''|]. \tag{A 6}$$

For the results shown in this work, (A 3) and (A 5) were evaluated for $D_{pm} = 0\,(Pe \to \infty)$.

https://doi.org/10.1017/jfm.2011.65 Published online by Cambridge University Press

Appendix B

Equation (2.15) can be further expanded in terms of the Eulerian velocity covariance, see (2.14), and the filter in (2.3), to account for sub-grid variability:

$$\begin{aligned} r_{ij}(t|\ell_p,\lambda_p) &= \frac{1}{2}\frac{\mathrm{d}}{\mathrm{d}t}\left[\frac{1}{\mathscr{V}_o^2}\int_{\mathscr{V}_o}\int_{\mathscr{V}_o}\int_0^t\int_0^t u_{ij}\left(\boldsymbol{r}\,|\boldsymbol{\beta},\lambda_p\right)\mathrm{d}t'\,\mathrm{d}t''\,\mathrm{d}\boldsymbol{a}'\,\mathrm{d}\boldsymbol{a}''\right] \\ &= \frac{1}{2\mathscr{V}_o^2}\frac{\mathrm{d}}{\mathrm{d}t}\int_{\mathscr{V}_o}\int_{\mathscr{V}_o}\int_0^t\int_0^t\int_{-\infty}^{\infty}\cdots\int_{-\infty}^{\infty} U_q U_p \\ &\quad\times\left(\delta_{iq}-\frac{k_i k_q}{k^2}\right)\left(\delta_{jn}-\frac{k_j k_n}{k^2}\right)\mathscr{F}(\boldsymbol{k}) \\ &\quad\times\hat{C}_Y(\boldsymbol{k})\exp[-\mathrm{i}\boldsymbol{k}\cdot(\boldsymbol{r}+\boldsymbol{\beta})]\,\mathrm{d}\boldsymbol{k}\,\mathrm{d}t'\,\mathrm{d}t''\,\mathrm{d}\boldsymbol{a}'\,\mathrm{d}\boldsymbol{a}'', \end{aligned} \tag{B 1}$$

which can be further expanded to

$$\begin{aligned} r_{ij}(t|\ell_p,\lambda_p) &= \frac{U_q U_p}{2\mathscr{V}_o^2}\frac{\mathrm{d}}{\mathrm{d}t}\int_{\mathscr{V}_o}\int_{\mathscr{V}_o}\int_0^t\int_0^t\int_{-\infty}^{\infty}\cdots\int_{-\infty}^{\infty}\left(\delta_{iq}-\frac{k_i k_q}{k^2}\right) \\ &\quad\times\left(\delta_{jn}-\frac{k_j k_n}{k^2}\right)\hat{C}_Y(\boldsymbol{k})\exp[-\mathrm{i}\boldsymbol{k}\cdot(\boldsymbol{r}+\boldsymbol{\beta})]\,\mathrm{d}\boldsymbol{k}\,\mathrm{d}t'\,\mathrm{d}t''\,\mathrm{d}\boldsymbol{a}'\,\mathrm{d}\boldsymbol{a}'' \\ &\quad-\frac{U_q U_p}{2\mathscr{V}_o^2}\frac{\mathrm{d}}{\mathrm{d}t}\int_{\mathscr{V}_o}\int_{\mathscr{V}_o}\int_0^t\int_0^t\int_{-\pi/\lambda_1}^{\pi/\lambda_1}\cdots\int_{-\pi/\lambda_m}^{\pi/\lambda_m}\left(\delta_{iq}-\frac{k_i k_q}{k^2}\right) \\ &\quad\times\left(\delta_{jn}-\frac{k_j k_n}{k^2}\right)\hat{C}_Y(\boldsymbol{k})\exp[-\mathrm{i}\boldsymbol{k}\cdot(\boldsymbol{r}+\boldsymbol{\beta})]\,\mathrm{d}\boldsymbol{k}\,\mathrm{d}t'\,\mathrm{d}t''\,\mathrm{d}\boldsymbol{a}'\,\mathrm{d}\boldsymbol{a}''. \end{aligned} \tag{B 2}$$

Appendix C

To obtain the result in (3.18), let

$$A = Y'(\boldsymbol{a}),\quad Z=\frac{1}{\ell_3}\int_0^{\ell_3} Y'(\boldsymbol{a})\,\mathrm{d}\boldsymbol{a},\quad W = Y'(\boldsymbol{a}''), \tag{C 1}$$

such that $\psi(\boldsymbol{a})\,\psi(\boldsymbol{a}'')$ in (3.17a) becomes

$$\begin{aligned} \int_0^{\ell_3}\int_0^{\ell_3}\psi(\boldsymbol{a}^{\mathrm{I}})\psi(\boldsymbol{a}^{\mathrm{II}})\,\mathrm{d}\boldsymbol{a}^{\mathrm{I}}\,\mathrm{d}\boldsymbol{a}^{\mathrm{II}} &= \int_0^{\ell_3}\int_0^{\ell_3}(A-Z)^2\,(W-Z)^2\,\mathrm{d}\boldsymbol{a}^{\mathrm{I}}\,\mathrm{d}\boldsymbol{a}^{\mathrm{II}} \\ &= \int_0^{\ell_3}\int_0^{\ell_3}(A^2W^2-2A^2WZ-2AW^2Z+A^2Z^2 \\ &\quad+4AWZ^2+W^2Z^2-2AZ^3-2WZ^3+Z^4)\,\mathrm{d}\boldsymbol{a}^{\mathrm{I}}\,\mathrm{d}\boldsymbol{a}^{\mathrm{II}}. \end{aligned} \tag{C 2}$$

The above equation can be further simplified by noticing that many of the terms are identical. By using the linear properties of the integral operator and expanding (C 2), we obtain the following:

$$\int_0^{\ell_3}\int_0^{\ell_3}A^2W^2\,\mathrm{d}\boldsymbol{a}^{\mathrm{I}}\,\mathrm{d}\boldsymbol{a}^{\mathrm{II}} = \int_0^{\ell_3}\int_0^{\ell_3}Y'^2(\boldsymbol{a}^{\mathrm{I}})Y'^2(\boldsymbol{a}^{\mathrm{II}})\,\mathrm{d}\mathbf{a}^{\mathrm{I}}\,\mathrm{d}\boldsymbol{a}^{\mathrm{II}}, \tag{C 3}$$

https://doi.org/10.1017/jfm.2011.65 Published online by Cambridge University Press

which represents θ_1 in (3.19). The integral in θ_2 from (3.19) is obtained from

$$\begin{aligned}\int_0^{\ell_3}\int_0^{\ell_3} A^2 W Z \,\mathrm{d}\boldsymbol{a}^{\mathrm{I}}\,\mathrm{d}\boldsymbol{a}^{\mathrm{II}} &= \int_0^{\ell_3}\int_0^{\ell_3} A W^2 Z \,\mathrm{d}\boldsymbol{a}^{\mathrm{I}}\,\mathrm{d}\boldsymbol{a}^{\mathrm{II}}\\ &= \int_0^{\ell_3}\int_0^{\ell_3} A^2 Z^2 \,\mathrm{d}\boldsymbol{a}^{\mathrm{I}}\,\mathrm{d}\boldsymbol{a}^{\mathrm{II}}\\ &= \int_0^{\ell_3}\int_0^{\ell_3} W^2 Z^2 \,\mathrm{d}\boldsymbol{a}^{\mathrm{I}}\,\mathrm{d}\boldsymbol{a}^{\mathrm{II}}\\ &= \frac{1}{\ell_3}\int_0^{\ell_3}\int_0^{\ell_3}\int_0^{\ell_3} Y'(\boldsymbol{a}^{\mathrm{I}})Y'^2(\boldsymbol{a}^{\mathrm{II}})Y'(\boldsymbol{a}^{\mathrm{III}})\,\mathrm{d}\boldsymbol{a}^{\mathrm{I}}\,\mathrm{d}\boldsymbol{a}^{\mathrm{II}}\,\mathrm{d}\boldsymbol{a}^{\mathrm{III}}. \quad (\mathrm{C}\,4)\end{aligned}$$

Finally, the integral in θ_3 arises from the integral below:

$$\begin{aligned}\int_0^{\ell_3}\int_0^{\ell_3} A W Z^2 \,\mathrm{d}\boldsymbol{a}^{\mathrm{I}}\,\mathrm{d}\boldsymbol{a}^{\mathrm{II}} &= \int_0^{\ell_3}\int_0^{\ell_3} A Z^3 \,\mathrm{d}\boldsymbol{a}^{\mathrm{I}}\,\mathrm{d}\boldsymbol{a}^{\mathrm{II}}\\ &= \int_0^{\ell_3}\int_0^{\ell_3} W Z^3 \,\mathrm{d}\boldsymbol{a}^{\mathrm{I}}\,\mathrm{d}\boldsymbol{a}^{\mathrm{II}}\\ &= \int_0^{\ell_3}\int_0^{\ell_3} Z^4 \,\mathrm{d}\boldsymbol{a}^{\mathrm{I}}\,\mathrm{d}\boldsymbol{a}^{\mathrm{II}}\\ = \frac{1}{\ell_3^2}\int_0^{\ell_3}\int_0^{\ell_3}\int_0^{\ell_3}\int_0^{\ell_3} Y'\left(\boldsymbol{a}^{\mathrm{I}}\right) Y'(\boldsymbol{a}^{\mathrm{II}})Y'(\boldsymbol{a}^{\mathrm{III}})Y'(\boldsymbol{a}^{\mathrm{IV}})\,\mathrm{d}\boldsymbol{a}^{\mathrm{I}}\,\mathrm{d}\boldsymbol{a}^{\mathrm{II}}\,\mathrm{d}\boldsymbol{a}^{\mathrm{III}}\,\mathrm{d}\boldsymbol{a}^{\mathrm{IV}}.\end{aligned} \quad (\mathrm{C}\,5)$$

Appendix D

Under the conditions stated in § 3.1 (e.g. fluctuating shear flow), we evaluate semi-closed forms of the integrals in ξ_0, ξ_1, ξ_2 and ξ_3 in Fourier space (accounting for the wiped-out variability). Starting with ξ_0 and using (3.22), we have

$$\xi_0 \equiv \rho_{\tilde{Y}}^2\left(0\,|\lambda\right) = \left\{1 - \mathrm{Erf}\left[\frac{I_v\sqrt{\pi}}{\lambda}\right]\right\}^2. \quad (\mathrm{D}\,1)$$

Let φ_1, φ_2 and φ_3 be auxiliary functions that represent the integrations of the functions present in ξ_1, ξ_2 and ξ_3 over ℓ_3, see (3.24*b*). We can now rewrite ξ_1 in Fourier space by using (3.22):

$$\xi_1 = \int_{-\infty}^{\infty}\int_{-\infty}^{\infty} \varphi_1\left(k_3,\kappa_3\right)\,\mathrm{d}k_3\,\mathrm{d}\kappa_3 - \int_{-\pi/\lambda}^{\pi/\lambda}\int_{-\pi/\lambda}^{\pi/\lambda} \varphi_1\left(k_3,\kappa_3\right)\,\mathrm{d}k_3\,\mathrm{d}\kappa_3, \quad (\mathrm{D}\,2)$$

with

$$\begin{aligned}\varphi_1\left(k_3,\kappa_3\right) = -&\frac{2I_v^2\exp\left[-I_v^2\left(k_3^2+\kappa_3^2\right)/\pi\right]}{\pi^2\left(k_3^2-\kappa_3^2\right)^2}\\ &\times\{(k_3^2+\kappa_3^2)[\cos(k_3^2\ell_3)\cos(\kappa_3^2\ell_3)-1]\\ &+2k_3^2\kappa_3^2\sin(k_3^2\ell_3)\sin(\kappa_3^2\ell_3)\}.\end{aligned} \quad (\mathrm{D}\,3)$$

Applying the same procedure for ξ_2 we obtain

$$\xi_2 = \Gamma_\infty - \int_{-\pi/\lambda}^{\pi/\lambda} \varphi_2\left(k_3\right)\,\mathrm{d}k_3, \quad (\mathrm{D}\,4)$$

https://doi.org/10.1017/jfm.2011.65 Published online by Cambridge University Press

with

$$\Gamma_\infty = 2I_v \left\{ \ell_3 \mathrm{Erf}\left(\frac{\sqrt{\pi}\ell_3}{2I_v} \right) + \frac{2I_v \left[\exp\left(-\frac{\pi \ell_3^2}{4I_v^2} \right) - 1 \right]}{\pi} \right\}, \tag{D 5}$$

and

$$\varphi_2(k_3) = \frac{2I_v \exp\left[-\frac{I_v^2 k_3^2}{\pi} \right] [1 - \cos(k_3 \ell_3)]}{\pi k_3^2}. \tag{D 6}$$

Finally, for ξ_3 we have

$$\xi_3 = \int_{-\infty}^{\infty} \int_{-\infty}^{\infty} \varphi_3(k_3, \kappa_3)\, \mathrm{d}k_3\, \mathrm{d}\kappa_3 - \int_{-\pi/\lambda}^{\pi/\lambda} \int_{-\pi/\lambda}^{\pi/\lambda} \varphi_3(k_3, \kappa_3)\, \mathrm{d}k_3\, \mathrm{d}\kappa_3, \tag{D 7}$$

where

$$\varphi_3(k_3, \kappa_3) = \frac{8I_v^2 \exp\left[-\frac{I_v^2 \left(k_3^2 + \kappa_3^2 \right)}{\pi} \right] \sin\left(\frac{k_1 \ell_3}{2} \right) \sin\left(\frac{\kappa_3 \ell_3}{2} \right)}{\pi^2 k_1 \kappa_3 \left(\kappa_3^2 - k_1^2 \right)} \times \left[\kappa_3 \cos\left(\frac{k_1 \ell_3}{2} \right) \sin\left(\frac{\kappa_3 \ell_3}{2} \right) - k_1 \sin\left(\frac{k_1 \ell_3}{2} \right) \cos\left(\frac{\kappa_3 \ell_3}{2} \right) \right]. \tag{D 8}$$

REFERENCES

Ababou, R., McLaughlin, D., Gelhar, L. W. & Tompson, A. F. B. 1989 Numerical simulation of three-dimensional saturated flow in randomly heterogeneous porous media. *Transp. Porous Media* **4** (6), 549–565.

Andricevic, R. & Cvetkovic, V. 1998 Relative dispersion for solute flux in aquifers. *J. Fluid Mech.* **361**, 145–174.

Attinger, S., Dentz, M., Kinzelbach, H. & Kinzelbach, W. 1999 Temporal behaviour of a solute cloud in a chemically heterogeneous porous medium. *J. Fluid Mech.* **386**, 77–104.

Attinger, S., Dentz, M. & Kinzelbach, W. 2004 Exact transverse macro dispersion coefficients for transport in heterogeneous porous media. *Stochastic Environ. Res. Risk Assessment* **18** (1), 9–15.

Auriault, J. L. & Adler, P. M. 1995 Taylor dispersion in porous media: analysis by multiple scale expansions. *Adv. Water Resour.* **18** (4), 217–226.

Batchelor, G. K. 1952 Diffusion in a field of homogeneous turbulence. II. The relative motion of particles. *Proc. Camb. Phil. Soc.* **48**, 345–362.

Beckie, R., Aldama, A. A. & Wood, E. F. 1996 Modeling the large-scale dynamics of saturated groundwater flow using spatial-filtering theory. 1. Theoretical development. *Water Resour. Res.* **32** (5), 1269–1280.

Bellin, A., Lawrence, A. E. & Rubin, Y. 2004 Models of sub-grid variability in numerical simulations of solute transport in heterogeneous porous formations: three-dimensional flow and effect of pore-scale dispersion. *Stochastic Environ. Res. Risk Assessment* **18** (1), 31–38.

Bellin, A., Salandin, P. & Rinaldo, A. 1992 Simulation of dispersion in heterogeneous porous formations: statistics, first-order theories, convergence of computations. *Water Resour. Res.* **28** (9), 2211–2227.

Bolster, D., Benson, D. A., Le Borgne, T. & Dentz, M. 2010 Anomalous mixing and reaction induced by superdiffusive nonlocal transport. *Phys. Rev.* E **82** (2), 21119.

https://doi.org/10.1017/jfm.2011.65 Published online by Cambridge University Press

Bolster, D., Dentz, M. & Le Borgne, T. 2009 Solute dispersion in channels with periodically varying apertures. *Phys. Fluids* **21**, 056601.

Bolster, D., Valdés-Parada, F. J., LeBorgne, T., Dentz, M. & Carrera, J. 2011 Mixing in confined stratified aquifers. *J. Contam. Hydrol.* **120–121**, 198–212.

Bras, R. L. & Rodríguez-Iturbe, I. 1994 *Random Functions and Hydrology*. Dover.

Chatwin, P. C. & Allen, C. M. 1985 Mathematical models of dispersion in rivers and estuaries. *Annu. Rev. Fluid Mech.* **17**, 119–149.

Chatwin, P. C. & Sullivan, P. J. 1979 The relative diffusion of a cloud of passive contaminant in incompressible turbulent flow. *J. Fluid Mech.* **91** (2), 337–355.

Cirpka, O. A. & Kitanidis, P. K. 2000 Characterization of mixing and dilution in heterogeneous aquifers by means of local temporal moments. *Water Resour. Res.* **36** (5), 1221–1136.

Cushman, J. H. & Moroni, M. 2001 Statistical mechanics with three-dimensional particle tracking velocimetry experiments in the study of anomalous dispersion. I. Theory. *Phys. Fluids* **13**, 75.

Cvetkovic, V. & Dagan, G. 1994 Transport of kinetically sorbing solute by steady random velocity in heterogenous porous formations. *J. Fluid Mech.* **265**, 189–215.

Cvetkovic, V., Dagan, G. & Cheng, H. 1998 Contaminant transport in aquifers with spatially variable hydraulic and sorption properties. *Proc. Math. Phys. Engng Sci.* **454** (1976), 2173–2207.

Cvetkovic, V. & Shapiro, A. M. 1989 Solute advection in stratified formations. *Water Resour. Res.* **25** (6), 1283–1289.

Dagan, G. 1984 Solute transport in heterogeneous porous formations. *J. Fluid Mech.* **145**, 151–177.

Dagan, G. 1987 Theory of solute transport by groundwater. *Annu. Rev. Fluid Mech.* **19**, 183–215.

Dagan, G. 1989 *Flow and Transport in Porous Formations*. Springer.

Dagan, G. 1990 Transport in heterogeneous porous formations: spatial moments, ergodicity & effective dispersion. *Water Resour. Res.* **26** (6), 1281–1290.

Dagan, G. 1991 Dispersion of a passive solute in non-ergodic transport by steady velocity fields in heterogeneous formations. *J. Fluid Mech.* **233**, 197–210.

Dagan, G. 1994 Transport by two-dimensional random velocity fields: effective dispersion coefficients of a finite plume. *Stochastic Meth. Hydrol. Environ. Engng* **2**, 113–126.

Dagan, G. & Fiori, A. 1997 The influence of pore-scale dispersion on concentration statistical moments in transport through heterogeneous aquifers. *Water Resour. Res.* **33** (7), 1595–1605.

Dagan, G., Fiori, A. & Jankovic, I. 2003 Flow and transport in highly heterogeneous formations. Part 1. Conceptual framework and validity of first-order approximations. *Water Resour. Res.* **39** (9), 1268.

Dentz, M. & Carrera, J. 2007 Mixing and spreading in stratified flow. *Phys. Fluids* **19**, 017107.

Dentz, M., Kinzelbach, H., Attinger, S. & Kinzelbach, W. 2000*a* Temporal behaviour of a solute cloud in a heterogeneous porous medium. 1. Point-like injection. *Water Resour. Res.* **36** (12), 3591–3604.

Dentz, M., Kinzelbach, H., Attinger, S. & Kinzelbach, W. 2000*b* Temporal behaviour of a solute cloud in a heterogeneous porous medium. 2. Spatially extended injection. *Water Resour. Res.* **36** (12), 3605–3614.

Dentz, M. & Tartakovsky, D. M. 2008 Self-consistent four-point closure for transport in steady random flows. *Phys. Rev.* E **77** (6), 66307.

de Dreuzy, J. R., Beaudoin, A. & Erhel, J. 2007 Asymptotic dispersion in 2D heterogeneous porous media determined by parallel numerical simulations. *Water Resour. Res.* **43**, W10439.

Eberhard, J. 2004 Approximations for transport parameters and self-averaging properties for point-like injections in heterogeneous media. *J. Phys.* A*: Math. Gen.* **37**, 2549–2571.

Eberhard, J. 2005 Upscaling for stationary transport in heterogeneous porous media. *Multiscale Model. Simulation (SIAM)* **3** (4), 957–976.

Elder, J. W. 1959 The dispersion of marked fluid in turbulent shear flow. *J. Fluid Mech.* **5** (4), 544–560.

Fiori, A. 1996 Finite Peclet extensions of Dagan's solutions to transport in anisotropic heterogeneous formations. *Water Resour. Res.* **32** (1), 193–198.

Fiori, A. 1998 On the influence of pore-scale dispersion in nonergodic transport in heterogeneous formations. *Transp. Porous Media* **30** (1), 57–73.

https://doi.org/10.1017/jfm.2011.65 Published online by Cambridge University Press

Fiori, A., Boso, F., de Barros, F. P. J., De Bartolo, S., Frampton, A., Severino, G., Suweis, S. & Dagan, G. 2010 An indirect assessment on the impact of connectivity of conductivity classes upon longitudinal asymptotic macrodispersivity. *Water Resour. Res.* **46** (8), W08601.

Fiori, A. & Dagan, G. 2000 Concentration fluctuations in aquifer transport: a rigorous first-order solution and applications. *J. Contam. Hydrol.* **45** (1–2), 139–163.

Fiori, A. & Dagan, G. 2002 Transport of a passive scalar in a stratified porous medium. *Transp. Porous Media* **47** (1), 81–98.

Fischer, H. B. 1973 Longitudinal dispersion and turbulent mixing in open-channel flow. *Annu. Rev. Fluid Mech.* **5** (1), 59–78.

Fischer, H. B., List, J. E., Koh, R. C. Y., Imberger, J. & Brooks, N. H. 1979 *Mixing in Inland and Coastal Waters*. Academic.

Gelhar, L. W. & Axness, C. L. 1983 Three-dimensional stochastic analysis of macrodispersion in aquifers. *Water Resour. Res.* **19** (1), 161–180.

Gotovac, H., Cvetkovic, V. & Andricevic, R. 2009 Flow and travel time statistics in highly heterogeneous porous media. *Water Resour. Res.* **45** (7), W07402.

Herrera, P. & Beckie, R. 2009 A new approach to model solute mixing in porous media. *Eos Trans. AGU Fall Meet. Suppl., Abstract H23D-0990* **90** (52).

Hou, Z. & Rubin, Y. 2005 On minimum relative entropy concepts and prior compatibility issues in vadose zone inverse and forward modeling. *Water Resour. Res.* **41** W12425.

Hsu, K. C., Zhang, D. & Neuman, S. P. 1996 Higher-order effects on flow and transport in randomly heterogeneous porous media. *Water Resour. Res.* **32** (3), 571–582.

Indelman, P. & Dagan, G. 1999 Solute transport in divergent radial flow through heterogeneous porous media. *J. Fluid Mech.* **384**, 159–182.

Jaynes, E. T. 1957 Information theory and statistical mechanics. *Phys. Rev.* **108** (2), 171–190.

Kitanidis, P. K. 1988 Prediction by the method of moments of transport in a heterogeneous formation. *J. Hydrol.* **102** (1–4), 453–473.

Koch, D. L. & Brady, J. F. 1988 Anomalous diffusion in heterogeneous porous media. *Phys. Fluids* **31**, 965.

Kraichnan, R. H. 1970 Diffusion by a random velocity field. *Phys. Fluids* **13**, 22.

Kramer, P. R., Majda, A. J. & Vanden-Eijnden, E. 2003 Closure approximations for passive scalar turbulence: a comparative study on an exactly solvable model with complex features. *J. Stat. Phys.* **111** (3), 565–679.

Kullback, S. 1997 *Information Theory and Statistics*. Dover.

Lawrence, A. E. & Rubin, Y. 2007 Block-effective macrodispersion for numerical simulations of sorbing solute transport in heterogeneous porous formations. *Adv. Water Resour.* **30** (5), 1272–1285.

Le Borgne, T., Dentz, M. & Carrera, J. 2008 Lagrangian statistical model for transport in highly heterogeneous velocity fields. *Phys. Rev. Lett.* **101** (9), 090601.

Majda, A. J. & Kramer, P. R. 1999 Simplified models for turbulent diffusion: theory, numerical modelling & physical phenomena. *Phys. Rep.* **314** (4–5), 237–574.

Matheron, G. & De Marsily, G. 1980 Is transport in porous media always diffusive: a counterexample. *Water Resour. Res.* **16** (5), 901–917.

McComb, W. D. 1990 *The Physics of Fluid Turbulence*. Clarendon Press.

Mole, N., Schopflocher, T. P. & Sullivan, P. J. 2008 High concentrations of a passive scalar in turbulent dispersion. *J. Fluid Mech.* **604**, 447–474.

Monin, A. S. & Yaglom, A. M. 1975 *Statistical Fluid Mechanics*, vol. 2. MIT Press.

Munro, R. J., Chatwin, P. C. & Mole, N. 2003 A concentration PDF for the relative dispersion of a contaminant plume in the atmosphere. *Boundary-Layer Meteorol.* **106** (3), 411–436.

Neuman, S. P. 1990 Universal scaling of hydraulic conductivities and dispersivities in geologic media. *Water Resour. Res.* **26** (8), 1749–1758.

https://doi.org/10.1017/jfm.2011.65 Published online by Cambridge University Press

Neuman, S. P. 2006 Blueprint for perturbative solution of flow and transport in strongly heterogeneous composite media using fractal and variational multiscale decomposition. *Water Resour. Res.* **42** (6), W06D04.

Neuman, S. P. & Zhang, Y. K. 1990 A quasi-linear theory of non-Fickian and Fickian subsurface dispersion. 1. Theoretical analysis with application to isotropic media. *Water Resour. Res.* **26** (5), 887–902.

Phythian, R. & Curtis, W. D. 1978 The effective long-time diffusivity for a passive scalar in a Gaussian model fluid flow. *J. Fluid Mech.* **89** (02), 241–250.

Rajaram, H. & Gelhar, L. W. 1993*a* Plume scale-dependent dispersion in heterogeneous aquifers 1. Lagrangian analysis in a stratified aquifer. *Water Resour. Res.* **29** (9), 3249–3260.

Rajaram, H. & Gelhar, L. W. 1993*b* Plume scale-dependent dispersion in heterogeneous aquifers 2. Eulerian analysis and three-dimensional aquifers. *Water Resour. Res.* **29** (9), 3261–3276.

Risken, H. 1989 *The Fokker-Planck Equation: Methods of Solution and Applications*, 2nd edn. Springer.

Rubin, Y. 1990 Stochastic modeling of macrodispersion in heterogeneous porous media. *Water Resour. Res.* **26** (1), 133–141.

Rubin, Y. 2003 *Applied Stochastic Hydrogeology*. Oxford University Press.

Rubin, Y., Bellin, A. & Lawrence, A. E. 2003 On the use of block-effective macrodispersion for numerical simulations of transport in heterogeneous formations. *Water Resour. Res.* **39** (9), 1242–1252.

Rubin, Y., Sun, A., Maxwell, R. & Bellin, A. 1999 The concept of block-effective macrodispersivity and a unified approach for grid-scale- and plume-scale-dependent transport. *J. Fluid Mech.* **395**, 161–180.

Sawford, B. 2001 Turbulent relative dispersion. *Annu. Rev. Fluid Mech.* **33** (1), 289–317.

Valocchi, A. J. 1990 Numerical simulation of the transport of adsorbing solutes in heterogeneous aquifers. In *Computational Methods in Subsurface Hydrology* (ed. G. Gambolati *et al.*), chap. 9, pp. 373–382. Computational Mechanics.

Woodbury, A. D. & Ulrych, T. J. 1993 Minimum relative entropy: forward probabilistic modeling. *Water Resour. Res.* **29** (8), 2847–2860.

Zavala-Sanchez, V., M. Dentz & Sanchez-Vila, X. 2009 Characterization of mixing and spreading in a bounded stratified medium. *Adv. Water Resour.* **32** (5), 635–648.

https://doi.org/10.1017/jfm.2011.65 Published online by Cambridge University Press